
Descent-Guided Policy Gradient for Scalable Cooperative Multi-Agent Learning

Shan Yang¹ Yang Liu^{2,1}

Abstract

Scaling cooperative multi-agent reinforcement learning (MARL) is fundamentally limited by cross-agent noise. When agents share a common reward, the actions of all N agents jointly determine each agent’s learning signal, so cross-agent noise grows with N . In the policy gradient setting, per-agent gradient estimate variance scales as $\Theta(N)$, yielding sample complexity $\mathcal{O}(N/\epsilon)$. We observe that many domains, including cloud computing, transportation, and power systems, have differentiable analytical models that prescribe efficient system states. In this work, we propose Descent-Guided Policy Gradient (DG-PG), a framework that utilizes these analytical models to provide each agent with a noise-free gradient signal, decoupling each agent’s gradient from the actions of all others. We prove that DG-PG reduces gradient variance from $\Theta(N)$ to $\mathcal{O}(1)$, preserves the equilibria of the cooperative game, and achieves agent-independent sample complexity $\mathcal{O}(1/\epsilon)$. On a heterogeneous cloud scheduling task with up to 200 agents, DG-PG converges within 10 episodes at every tested scale, from $N=5$ to $N=200$, directly confirming the predicted scale-invariant complexity, while MAPPO and IPPO fail to converge under identical architectures.

1. Introduction

Multi-agent reinforcement learning (MARL) has demonstrated remarkable success across a wide range of domains, from game playing (Yu et al., 2022) to cloud resource scheduling (Mao et al., 2019) and transportation management (El-Tantawy et al., 2013). In many of these applications, agents share a common objective and must coordinate

their behavior, a setting known as cooperative MARL. However, scaling cooperative MARL remains a fundamental challenge, as performance degrades sharply with the number of agents. The root of this difficulty is *multi-agent credit assignment*: when all agents share a single reward signal, it becomes increasingly hard to determine how much each agent’s action contributed to the observed outcome, and this ambiguity worsens with every additional agent.

Concretely, any optimization signal in cooperative MARL, whether a policy gradient, a Q-value, or an advantage estimate, must be derived from a shared return that aggregates the actions of all N agents, introducing cross-agent noise that grows linearly with N . Kuba et al. (2021) formalize this in the policy gradient setting, showing that the variance of each agent’s gradient estimate scales as $\Theta(N)$, implying sample complexity $\mathcal{O}(N/\epsilon)$ and a signal-to-noise ratio that decays as $1/\sqrt{N}$. The central bottleneck in scaling cooperative MARL is thus the cross-agent noise inherent to learning from shared rewards.

Existing approaches attempt to mitigate cross-agent noise through two broad strategies. The first is credit decomposition, extracting per-agent contributions from the shared return via counterfactual baselines (Foerster et al., 2018), value factorization (Rashid et al., 2020; Wang et al., 2021), or marginal contribution estimation (Wolpert & Tumer, 2001). These methods reduce but do not eliminate cross-agent noise, as the learning signal remains derived from the shared return. The second strategy incorporates pre-designed controllers as base policies (Levine & Koltun, 2013; Johannink et al., 2019), providing a noise-free action component. However, this constrains the learned policy near the controller, which may prevent it from reaching the true optimum. In both cases, cross-agent noise is either reduced but not eliminated, or avoided at the cost of constraining the solution space.

We observe that many cooperative systems already possess an underexploited source of noise-free per-agent signals. For example, in domains such as cloud scheduling, traffic routing, and power dispatch, differentiable analytical models have been developed over decades in operations research and control theory. These models typically rely on simplifying assumptions and global system information, and thus cannot be directly translated into executable policies for

¹Department of Industrial Systems Engineering and Management, National University of Singapore, Singapore ²Department of Civil and Environmental Engineering, National University of Singapore, Singapore. Correspondence to: Yang Shan <yang_shan@u.nus.edu>, Liu Yang <ceelya@nus.edu.sg>.

individual agents. However, their differentiable structure can provide each agent with a noise-free gradient signal that depends only on the agent’s own influence on the system state.

Building on this insight, we propose Descent-Guided Policy Gradient (DG-PG), a framework that integrates such analytical models into cooperative policy optimization. Our key contributions are:

- **Framework.** We augment the policy gradient with the gradient of a differentiable guidance term derived from analytical models. Crucially, the differentiable structure of these models allows this gradient to isolate each agent’s individual contribution to the system state, yielding a noise-free signal computable without any other agent’s action. The framework requires no architectural changes to existing actor-critic methods.
- **Theoretical guarantees.** We prove three properties under mild structural assumptions: (i) the augmented gradient does not alter the Nash equilibria of the original cooperative game (Theorem 4.1); (ii) the per-agent gradient estimate variance reduces from $\Theta(N)$ to $\mathcal{O}(1)$, independent of the number of agents (Theorem 4.2); and (iii) the sample complexity to reach an ϵ -optimal solution is $\mathcal{O}(1/\epsilon)$, also independent of N (Theorem 4.3).
- **Empirical validation.** We evaluate DG-PG on heterogeneous cloud resource scheduling with up to $N=200$ agents, where standard multi-agent policy gradient methods fail to converge. DG-PG achieves stable learning across all scales, consistently outperforming MAPPO and IPPO with significantly fewer training episodes.

2. Preliminaries

We consider a fully cooperative MARL setting, formalized as a *Cooperative Markov Game* (equivalently, a Dec-POMDP) (Oliehoek & Amato, 2016). The game is defined by the tuple $\mathcal{M} = \langle \mathcal{N}, \mathcal{S}, \mathcal{A}, P, r, \gamma \rangle$, where $\mathcal{N} = \{1, \dots, N\}$ denotes the set of N agents, \mathcal{S} is the global state space, and $\mathcal{A} = \times_{i \in \mathcal{N}} \mathcal{A}^i$ is the joint action space with \mathcal{A}^i representing the action space for agent i . At each timestep t , the system is in state $s_t \in \mathcal{S}$. Each agent i receives a local observation o_t^i (derived from s_t) and selects an action $a_t^i \in \mathcal{A}^i$ according to its policy $\pi_{\theta^i}(a_t^i | o_t^i)$, parameterized by θ^i . The environment then transitions to state s_{t+1} according to the dynamics $P(s_{t+1} | s_t, \mathbf{a}_t)$, where $\mathbf{a}_t = (a_t^1, \dots, a_t^N)$ denotes the joint action.

2.1. Cooperative Objective and Policy Gradient

In the cooperative setting, all agents share a common global reward function $r(s_t, \mathbf{a}_t)$. The shared objective is to maxi-

mize the expected discounted cumulative reward:

$$J(\boldsymbol{\theta}) = \mathbb{E}_{\pi} \left[\sum_{t=0}^{\infty} \gamma^t r(s_t, \mathbf{a}_t) \right], \quad (1)$$

where $\gamma \in [0, 1)$ is the discount factor and π denotes the joint policy. Standard policy gradient methods perform gradient ascent on $J(\boldsymbol{\theta})$. For agent i , the gradient with respect to its parameters θ^i is given by the Policy Gradient Theorem (Sutton et al., 1999):

$$\nabla_{\theta^i} J(\boldsymbol{\theta}) = \mathbb{E}_{\pi} \left[\sum_{t=0}^{\infty} \gamma^t \nabla_{\theta^i} \log \pi_{\theta^i}(a_t^i | o_t^i) R_t \right], \quad (2)$$

where $R_t = \sum_{k=0}^{\infty} \gamma^k r_{t+k}$ is the sampled return from time t .

2.2. The Variance Explosion Problem

While Equation 2 provides an unbiased gradient estimator, its variance poses a critical challenge in large-scale settings. Because the estimator relies on sampled returns that depend on the joint action \mathbf{a}_t of all N agents, each agent’s gradient estimate carries noise from every other agent’s sampled actions. Following Kuba et al. (2021), this variance can be decomposed as:

$$\text{Var}(\hat{g}^i) \approx \underbrace{\sigma_{\text{self}}^2}_{\text{Own Exploration}} + \underbrace{(N-1)\sigma_{\text{others}}^2}_{\text{Cross-Agent Noise}}. \quad (3)$$

The second term represents the noise from sampling other agents’ actions. As N increases, this term dominates, causing the total estimation variance to scale as $\Theta(N)$. This linear scaling implies that maintaining a constant estimation error requires the batch size to grow linearly with N , rendering *standard multi-agent policy gradient methods sample-inefficient for large-scale systems*.

Existing variance reduction techniques, such as state-value baselines $V(s)$ or counterfactual baselines like COMA (Foster et al., 2018), primarily target the self-exploration term σ_{self}^2 . While effective in smaller settings, their ability to mitigate the $\Theta(N)$ cross-agent noise term diminishes in large-scale systems without incurring significant computational overhead. Similarly, mean-field methods (Yang et al., 2018) offer scalability but require agents to be exchangeable and homogeneous, assumptions that do not hold in domains such as cloud scheduling, power grids, and traffic networks, where agents have *heterogeneous capacities* and *structured coupling constraints*.

3. Method: Descent-Guided Policy Gradient

In this section, we present DG-PG, a framework that addresses the variance explosion problem by exploiting the

analytical models available in many cooperative domains. We first define the *reference state* as an efficient system state prescribed by analytical models and identify the conditions under which it yields a valid guidance term (Section 3.1). We then augment the policy gradient with a noise-free, per-agent signal derived from the reference (Section 3.2). Under mild assumptions, DG-PG does not alter the Nash equilibria of the original cooperative game while achieving agent-independent variance.

3.1. Utilizing Analytical Priors: System State and Reference

In many cooperative domains, analytical models from operations research and control theory, such as fluid-limit approximations for queueing systems, equilibrium analysis for traffic networks, or convex optimization for resource allocation, provide principled characterizations of desirable system behavior. While not executable under real-world stochasticity, these models offer something valuable, namely a *reference* that describes what efficient system operation looks like under given conditions. Our key observation is that such a reference, if properly defined, can supply each agent with a clear, directed signal for policy improvement. This signal is far more informative than the noisy scalar reward r_t aggregated over all agents.

As noted above, domain-specific models can prescribe efficient system states, but these states must be expressed in a concrete representational space. We define a *system state* $\mathbf{x}_t \in \mathbb{R}^m$ as the vector of system-level quantities jointly determined by agents' actions (e.g., per-server resource utilization, per-link flow, or queue lengths), where m is the number of monitored quantities. The *reference state* $\tilde{\mathbf{x}}_t \in \mathbb{R}^m$ is the efficient state that the analytical model yields under current conditions, computed independently of the learned policies. A key structural property of \mathbf{x}_t is that each agent's action typically affects only specific dimensions of this vector, so that each agent's influence on the system state is localized. We exploit this property in the gradient computation (Section 3.2).

For the reference to yield a valid guidance signal, it should ideally satisfy two conditions:

Assumption 3.1 (Exogeneity). The reference trajectory $\tilde{\mathbf{x}}_t$ is non-adaptive with respect to the policy parameters:

$$\nabla_{\theta} \tilde{\mathbf{x}}_t = \mathbf{0}. \quad (4)$$

Assumption 3.2 (Descent-Aligned Reference). Moving the system state toward the reference improves system performance. Formally, for any $\mathbf{x}_t \neq \tilde{\mathbf{x}}_t$:

$$\langle \nabla_{\mathbf{x}} J(\mathbf{x}_t), \tilde{\mathbf{x}}_t - \mathbf{x}_t \rangle > 0. \quad (5)$$

When both conditions hold, the reference provides a stable, directionally correct target that does not shift as policies

update (Assumption 3.1), and approaching it is expected to improve the cooperative objective (Assumption 3.2). This means that any mechanism that steers the system state toward $\tilde{\mathbf{x}}_t$ is aligned with the original optimization goal, a property we exploit in the next subsection to construct a low-variance gradient estimator. Both assumptions are broadly satisfied in structured cooperative domains and can be approximately verified in practice. We verify both assumptions concretely for the cloud scheduling setting in Appendix C.

Importantly, $\tilde{\mathbf{x}}_t$ need not be reachable by the agents, because it may arise from idealized fluid-limit or steady-state models. DG-PG uses $\tilde{\mathbf{x}}_t$ only to define a descent direction, not as a target to be attained exactly.

3.2. Descent-Guided Policy Gradient

Given a reference $\tilde{\mathbf{x}}_t$ satisfying Assumptions 3.1–3.2, steering the system toward $\tilde{\mathbf{x}}_t$ at each step is directionally aligned with improving J . The challenge is to incorporate this information into the learning process in a way that (i) does not alter the original cooperative objective, and (ii) provides each agent with a gradient signal free of cross-agent noise. Our DG-PG achieves both by exploiting the differentiable structure of these models at the gradient level, providing each agent with its own noise-free update direction.

Concretely, we construct the DG-PG framework in three steps. We first define a deviation measure that quantifies the gap between the current system state and the reference. We then differentiate this measure through each agent's action to obtain a per-agent descent direction. Finally, we use these directions to guide the standard policy gradient, thus eliminating cross-agent noise.

Deviation Measure. We first define a per-step deviation function to quantify how far the system state deviates from the reference:

$$d(\mathbf{x}_t, \tilde{\mathbf{x}}_t) = \frac{1}{2} \|\mathbf{x}_t - \tilde{\mathbf{x}}_t\|^2. \quad (6)$$

By Assumption 3.2, reducing d at each step is directionally consistent with improving J . However, simply incorporating d into the reward would yield a scalar signal that cannot distinguish each agent's individual effect. Since d is differentiable with respect to \mathbf{x}_t and \mathbf{x}_t depends differentially on each a_t^i , the gradient $\partial d / \partial a_t^i$ can be computed analytically. Thus, the gradient of d can serve as a guidance signal for each agent, aligned with improving J .

DG-PG Gradient. We augment the standard policy gradient with the gradient of d , yielding the DG-PG gradient:

$$\nabla_{\theta^i} J_{\alpha} \triangleq (1 - \alpha) \nabla_{\theta^i} J - \alpha \nabla_{\theta^i} \mathcal{G}, \quad (7)$$

where $\alpha \in (0, 1)$ is the guidance weight, and $\mathcal{G} \triangleq \mathbb{E}_{s \sim \nu, \pi} [d(\mathbf{x}_t, \tilde{\mathbf{x}}_t)]$ is the expected deviation under the state

visitation distribution ν^π induced by the joint policy. The DG-PG gradient $\nabla_{\theta^i} J_\alpha$ thus retains the optimization direction of J while incorporating a guidance signal from the reference model. We prove that this augmentation preserves the Nash equilibria of the original game (Theorem 4.1).

To evaluate $\nabla_{\theta^i} \mathcal{G}$, we apply the chain rule through \mathbf{x}_t to isolate each agent’s contribution to the deviation:

$$\frac{\partial d}{\partial a_t^i} = \left\langle \nabla_{\mathbf{x}} d, \frac{\partial \mathbf{x}_t}{\partial a_t^i} \right\rangle = \langle \mathbf{x}_t - \tilde{\mathbf{x}}_t, \mathbf{z}_t^i \rangle, \quad (8)$$

where $\mathbf{z}_t^i \triangleq \frac{\partial \mathbf{x}_t}{\partial a_t^i}$ is agent i ’s *local influence vector*, the partial derivative of the system state with respect to its action. This coefficient measures the deviation projected onto the dimensions that agent i influences. It depends only on the current state \mathbf{x}_t , the exogenous reference $\tilde{\mathbf{x}}_t$, and the agent-local derivative \mathbf{z}_t^i , so it carries no cross-agent noise and can be computed analytically. The concrete form of \mathbf{z}_t^i depends on the domain, and we derive it for cloud scheduling in Appendix D.

Substituting Equation 8 into the policy gradient theorem yields the gradient of the guidance term:

$$\nabla_{\theta^i} \mathcal{G} = \mathbb{E}_{s \sim \nu^\pi, \mathbf{a} \sim \pi} [\langle \mathbf{x}_t - \tilde{\mathbf{x}}_t, \mathbf{z}_t^i \rangle \nabla_{\theta^i} \log \pi^i(a_t^i | o_t^i)]. \quad (9)$$

Gradient Estimator. In practice, we estimate the DG-PG gradient $\nabla_{\theta^i} J_\alpha$ via the score function method. At each step t of a sampled trajectory, the gradient estimate for agent i is:

$$\hat{g}_{\text{DG},t}^i = (1 - \alpha) \hat{g}_{J,t}^i - \alpha \hat{g}_{\mathcal{G},t}^i, \quad (10)$$

where

$$\hat{g}_{J,t}^i = R_t \nabla_{\theta^i} \log \pi^i(a_t^i | o_t^i), \quad (11)$$

$$\hat{g}_{\mathcal{G},t}^i = \langle \mathbf{x}_t - \tilde{\mathbf{x}}_t, \mathbf{z}_t^i \rangle \nabla_{\theta^i} \log \pi^i(a_t^i | o_t^i). \quad (12)$$

Each agent then updates its policy parameters via gradient ascent:

$$\theta_{k+1}^i = \theta_k^i + \eta \hat{g}_{\text{DG},t}^i, \quad (13)$$

where $\eta > 0$ is the learning rate.

Variance Properties. The two components of $\hat{g}_{\text{DG},t}^i$ have fundamentally different variance properties. The standard policy gradient sample $\hat{g}_{J,t}^i$ uses the return R_t , which aggregates all N agents’ stochastic actions, yielding $\Theta(N)$ variance. The guidance sample $\hat{g}_{\mathcal{G},t}^i$ uses an analytically computed coefficient $\langle \mathbf{x}_t - \tilde{\mathbf{x}}_t, \mathbf{z}_t^i \rangle$, contributing $\mathcal{O}(1)$ variance independent of N . We formalize how the choice of α controls this variance trade-off in Section 4.

3.3. Implementation

Integration with MAPPO. DG-PG can be integrated into the MAPPO framework (Yu et al., 2022) by modifying the advantage estimator. After collecting trajectories and computing the standard GAE advantages $\hat{A}_{\text{GAE}}^i(t)$, they are augmented with the guidance term:

$$\hat{A}_{\text{DG}}^i(t) = (1 - \alpha) \hat{A}_{\text{GAE}}^i(t) - \alpha \cdot \langle \mathbf{x}_t - \tilde{\mathbf{x}}_t, \mathbf{z}_t^i \rangle, \quad (14)$$

The policy and critic are then updated using standard PPO objectives with the modified advantages. The computational overhead is minimal, since the reference trajectory $\{\tilde{\mathbf{x}}_t\}$ is computed once per batch from the analytical model, and each guidance coefficient amounts to an $\mathcal{O}(m)$ inner product per agent.

Comparison with Existing Methods. Unlike counterfactual methods (e.g., COMA (Foerster et al., 2018)) that require training N separate critics to marginalize each agent’s action, or value decomposition methods (e.g., QMIX (Rashid et al., 2020)) that need additional mixing networks, DG-PG requires *no architectural changes* to the actor-critic framework. The entire modification amounts to a single line adjusting the advantage estimator. This simplicity is enabled by our analytical gradient computation (Section 3.2), which directly provides per-agent credit assignment without requiring learned components.

4. Theoretical Guarantees

In this section, we establish the theoretical foundations of DG-PG. Our central result is that the DG-PG gradient estimator achieves *agent-independent variance* (Theorem 4.2), breaking the $\Theta(N)$ scaling barrier of standard policy gradients. We complement this with two supporting guarantees: (1) *consistency* (Theorem 4.1), ensuring that DG-PG preserves the Nash equilibria of the original game; and (2) *sample complexity* (Theorem 4.3), showing that the variance reduction yields agent-independent convergence rates under standard regularity assumptions (the complete dependency structure is given in Table 3, Appendix B).

4.1. Nash Invariance

A primary concern when augmenting the policy gradient is whether the additional guidance term shifts the Nash equilibria of the original cooperative game. We prove that under our assumptions, $\nabla_{\theta^i} J_\alpha$ vanishes at every Nash equilibrium of J .

Theorem 4.1 (Nash Invariance). *Let θ^* be a Nash equilibrium of the original cooperative game, i.e., $\nabla_{\theta^i} J(\theta^*) = \mathbf{0}$ for all $i \in \mathcal{N}$. Under Assumptions 3.1–3.2, the DG-PG gradient also vanishes at θ^* :*

$$\nabla_{\theta^i} J_\alpha(\theta^*) = \mathbf{0}, \quad \forall \alpha \in (0, 1), \forall i \in \mathcal{N}. \quad (15)$$

This result guarantees the *safety* of DG-PG, as the augmentation of the guidance term does not alter the Nash equilibria of the original game.

Proof Sketch. We first show by contradiction that $\nabla_{\theta^i} \mathcal{G}(\theta^*) = \mathbf{0}$ at any Nash equilibrium θ^* (Lemma E.1). Since both $\nabla_{\theta^i} J$ and $\nabla_{\theta^i} \mathcal{G}$ vanish at θ^* , the DG-PG gradient $\nabla_{\theta^i} J_\alpha = (1 - \alpha) \cdot \mathbf{0} - \alpha \cdot \mathbf{0} = \mathbf{0}$. The detailed proof is in Appendix E. \square

4.2. Variance Reduction

Having established that DG-PG preserves the Nash equilibria of J (Theorem 4.1), we now formalize the variance properties of the DG-PG gradient estimator. The return R_t in the standard policy gradient aggregates all N agents’ stochastic actions, so the per-agent gradient variance $\text{Var}(\hat{g}_J^i) = \Theta(N)$. In contrast, the guidance coefficient $\langle x_t - \tilde{x}_t, z_t^i \rangle$ depends only on agent-local quantities (Section 3.2), yielding guidance gradient variance $\text{Var}(\hat{g}_G^i) = \mathcal{O}(1)$ independent of N .

Since the DG-PG estimator combines \hat{g}_J^i and \hat{g}_G^i , the combined variance depends on their correlation $\rho = \text{Corr}(\hat{g}_J^i, \hat{g}_G^i)$. Under Assumption 3.2, improving J reduces the deviation \mathcal{G} , so \hat{g}_J^i and \hat{g}_G^i are negatively correlated ($\rho < 0$). The following theorem characterizes the optimal variance as a function of ρ and the variances of two gradient estimators.

Theorem 4.2 (Agent-Independent Variance Bound). *Under Assumptions 3.1–3.2, let $\sigma_J^2 \triangleq \text{Var}(\hat{g}_J^i)$, $\sigma_G^2 \triangleq \text{Var}(\hat{g}_G^i)$, and $\rho \triangleq \text{Corr}(\hat{g}_J^i, \hat{g}_G^i) \in (-1, 0)$. The optimally weighted combined estimator achieves:*

$$\min_{\alpha \in (0,1)} \text{Var}(\hat{g}_{\text{DG}}^i) = \frac{\sigma_J^2 \sigma_G^2 (1 - \rho^2)}{\sigma_J^2 + \sigma_G^2 + 2\rho \sigma_J \sigma_G}. \quad (16)$$

Since $\sigma_J^2 = \Theta(N)$ and $\sigma_G^2 = \mathcal{O}(1)$ (established above), the minimum variance satisfies $\min_\alpha \text{Var}(\hat{g}_{\text{DG}}^i) = \mathcal{O}(1)$ for all N , independent of the number of agents.

Proof Sketch. The combined variance $\sigma_{\text{DG}}^2(\alpha)$ is a convex quadratic in α with cross-term $\rho \sigma_J \sigma_G$. Minimizing in closed form yields

$$\sigma_{\text{DG},\min}^2 = \sigma_G^2(1 - \rho^2) / (\sigma_J^2 + \sigma_G^2 + 2\rho \sigma_J \sigma_G).$$

Substituting $\sigma_J^2 = \Theta(N)$ and $\sigma_G^2 = \mathcal{O}(1)$, the denominator is dominated by σ_J^2 and is thus bounded away from zero, while the numerator is $\mathcal{O}(1)$, giving $\sigma_{\text{DG},\min}^2 = \mathcal{O}(1)$ for all N . The corresponding optimal weight α^* satisfies $\alpha^* \rightarrow 1$ as N grows, indicating that larger systems rely more on the guidance signal. The full derivation is provided in Appendix F. \square

The role of α . Although $\alpha^* \rightarrow 1$ is optimal in the large- N limit, two practical factors prevent setting α close to 1. First, since the score function $\nabla \log \pi^i$ introduces irreducible stochasticity that does not vanish with N , the guidance variance σ_G^2 persists. Second, in many practical domains, Assumptions 3.1–3.2 may not hold exactly, in which case the Nash invariance guarantee (Theorem 4.1) may no longer hold. Consequently, the choice of α must balance variance reduction against fidelity to the original game. We investigate the sensitivity to α and the effect of scheduling strategies empirically in Section 6.

4.3. Convergence Rate

The variance reduction in Theorem 4.2, combined with standard regularity assumptions, yields agent-independent sample complexity.

Theorem 4.3 (Sample Complexity). *Assume J is L -smooth and satisfies the Polyak-Łojasiewicz (PL) condition with PL constant $\mu \in (0, L]$ (see Assumption G.1 in Appendix G). Under the variance bound from Theorem 4.2, DG-PG achieves an ϵ -optimal policy in:*

$$T = \mathcal{O} \left(\frac{L}{\mu^2 \epsilon} \log \frac{1}{\epsilon} \right) \quad (17)$$

iterations. This bound is independent of the number of agents N .

This result establishes that DG-PG’s convergence rate is independent of the number of agents, so adding more agents does not require additional training iterations. In contrast, standard multi-agent policy gradient methods require $T = \mathcal{O}(N/\epsilon)$ iterations to compensate for $\Theta(N)$ variance.

Proof Sketch. L -smoothness bounds the per-iteration descent in terms of $\|\nabla J\|^2$ and the gradient variance σ_{DG}^2 . The PL condition then converts $\|\nabla J\|^2$ into the optimality gap $J^* - J(\theta_k)$. Substituting $\sigma_{\text{DG}}^2 = \mathcal{O}(1)$ from Theorem 4.2 yields the N -independent bound. The full derivation is provided in Appendix G. \square

Summary. Theorems 4.1–4.3 collectively establish that DG-PG is (1) scalable: variance does not grow with N ; (2) safe: optimal solutions are preserved; and (3) efficient: sample complexity is agent-independent.

5. Related Work

Credit Assignment in Cooperative MARL. Credit decomposition methods attempt to extract per-agent contributions from the shared return. Difference Rewards (Wolpert & Tumer, 2001) isolate each agent’s marginal contribution via counterfactual simulation, but require access to the reward function or a simulator. Value decomposition methods,

such as VDN (Sunehag et al., 2017), QMIX (Rashid et al., 2020), and QPLEX (Wang et al., 2021), factorize the joint Q-function into per-agent terms under structural assumptions (additivity, monotonicity), avoiding gradient estimation but restricting the class of representable objectives. COMA (Foerster et al., 2018) trains a centralized critic to compute counterfactual baselines that marginalize each agent’s action, but the critic must condition on the joint action space and becomes difficult to train as N grows. All these methods still derive their training signal from the shared return, so the cross-agent noise that grows with N persists.

Variance Reduction in Multi-Agent Policy Gradients.

Standard variance reduction techniques, including value function baselines (Sutton & Barto, 1998) and GAE (Schulman et al., 2016), primarily reduce temporal variance from an agent’s own stochasticity. In the multi-agent setting, HAPPO (Kuba et al., 2022) reduces cross-agent noise by updating agents sequentially, conditioning each agent’s update on the previous agents’ new policies. This is effective but sacrifices parallel execution, as each agent must wait for all preceding updates. Agent-specific baselines can reduce the self-exploration component of variance but do not explicitly target the cross-agent noise that dominates in large-scale settings. Mean-Field MARL (Yang et al., 2018) takes a different approach, replacing the N -agent interaction with a population-level approximation that simplifies each agent’s optimization problem. This achieves scalability but requires agent homogeneity, precluding application to heterogeneous settings.

Reward Shaping. Potential-Based Reward Shaping (PBRS) (Ng et al., 1999) shares with DG-PG the property of preserving optimal policies, but the two operate at different levels. PBRS reshapes the scalar reward via a potential function to provide denser temporal feedback, accelerating single-agent exploration. However, the shaped reward still aggregates all agents’ actions, so the resulting gradient estimator retains $\Theta(N)$ cross-agent variance. DG-PG instead operates at the gradient level, augmenting each agent’s policy gradient with a signal computed analytically from the reference model.

Structural Priors in RL. Guided Policy Search (Levine & Koltun, 2013) and Residual RL (Johannink et al., 2019) incorporate domain knowledge by using pre-computed controllers as base policies or supervisory signals, but this couples the learned policy to the quality of the prior and can bias the solution. Physics-Informed Neural Networks (Raissi et al., 2019) embed governing equations directly into the loss function, but require exact PDEs and do not decompose across agents. DG-PG uses analytical models differently, constructing noise-free per-agent gradients of a guidance term that reduce gradient estimate variance without altering the optimization landscape. A systematic comparison is provided in Appendix A.

6. Experiments

We evaluate DG-PG on heterogeneous cloud scheduling across scales from $N=5$ to $N=200$, a challenging domain where queueing-theoretic priors are readily available and the cross-agent noise problem is particularly acute. Our experiments address three questions: (1) sensitivity to the guidance weight α ; (2) controlled comparison against MAPPO and IPPO under identical training configurations; (3) scalability to large agent populations where standard methods fail.

6.1. Setup

Environment. We evaluate on a heterogeneous cloud scheduling simulator with N servers whose configurations are based on AWS instance types. The environment combines three sources of complexity (heterogeneous server efficiency, bimodal workloads with heavy tails, and non-stationary arrivals) that jointly violate the stationarity assumptions of the queueing-theoretic prior, testing robustness to model mismatch. The reward balances two competing objectives: latency (queue minimization) and energy efficiency (preferring high- η_{CPU} servers), which cannot be simultaneously optimized by simple heuristics. Figure 1 illustrates these characteristics. We evaluate at scales $N \in \{5, 10, 20, 50, 100, 200\}$. For each scale, we pre-generate 200 training scenarios and 40 held-out test scenarios with randomized server configurations and workload patterns. Full specifications are in Appendix H.

Baselines. We compare against (1) **MAPPO** (Yu et al., 2022), multi-agent PPO with a centralized value function (CTDE), and (2) **IPPO**, independent PPO with local value functions. Both share the same actor-critic backbone as DG-PG and execute decentrally from local observations; any performance gap therefore isolates the effect of gradient guidance. We additionally report (3) **Best-Fit**, a resource-aware greedy heuristic that operates with full global state, as a centralized upper reference, and (4) **Random** as a lower reference. Mean-Field methods (Yang et al., 2018) are excluded because they assume agent homogeneity, which is violated by our heterogeneous server setting. Training hyperparameters for all methods are detailed in Appendix I.

6.2. Hyperparameter Selection

The guidance weight $\alpha \in (0, 1)$ controls the bias-variance trade-off in DG-PG. Larger α reduces gradient variance by relying more heavily on the analytical prior, while smaller α maintains closer alignment with the true reward signal. We conduct a systematic grid search over $\alpha \in \{0.2, 0.4, 0.6, 0.8\}$ at $N = 50$ using NN models, with validation at $N = 20$.

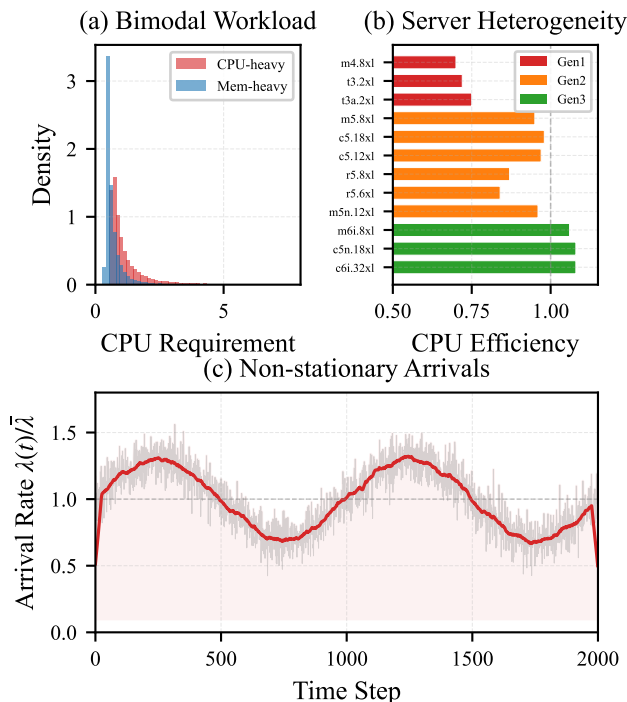


Figure 1. **Environment characteristics.** (a) Bimodal workload distribution: CPU-intensive jobs (60%, Pareto $\alpha=1.7$) and memory-intensive jobs (40%, Pareto $\alpha=2.2$) with heavy tails. (b) Server heterogeneity across three hardware generations with CPU efficiency spanning 0.70–1.08. (c) Non-stationary job arrival rate with tidal fluctuation (period = 1000 steps) and Gaussian noise.

Results. Figure 2 shows training curves at $N=50$ for all tested α values. The results reveal a clear trade-off in which *larger α accelerates early convergence, while smaller α achieves marginally superior final performance*. By episode 200, $\alpha=0.2$ achieves the best mean training reward of -40.3 , while $\alpha=0.8$ reaches -40.8 , a gap of less than 1%. This trend is consistent at $N=20$, where $\alpha=0.2$ achieves -39.9 . The narrow spread across α values demonstrates that DG-PG is *robust to the choice of α* , as the RL gradient compensates for model inaccuracy while benefiting from variance reduction at any tested setting.

Selected Hyperparameters. Based on the observed trade-off, we adopt a *dynamic α scheduling strategy*: initialize with $\alpha=0.9$ for the first 10% of training to leverage fast early convergence, then linearly decay to $\alpha=0.2$ over the next 40% of training, and maintain $\alpha=0.2$ for the remainder. This exploits the strong guidance signal for rapid initial progress while preserving the policy’s capacity for fine-tuning. All subsequent experiments use this schedule.

6.3. Controlled Comparison

To isolate the effect of gradient guidance, all three methods are compared under identical core training configurations

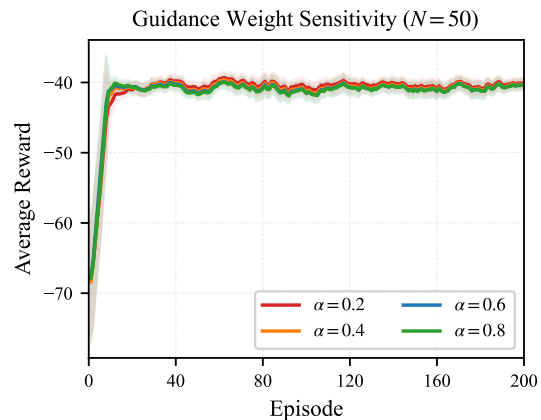


Figure 2. **Hyperparameter sensitivity.** Training reward at $N=50$ for varying guidance weight $\alpha \in \{0.2, 0.4, 0.6, 0.8\}$. All values converge rapidly and achieve similar final performance, confirming robustness to α .

(Appendix I). MAPPO and IPPO additionally receive $2.5\times$ more training (500 vs. 200 episodes) and individually tuned entropy coefficients to enhance their convergence stability. We restrict this comparison to small scales $N \in \{2, 5, 10\}$, where gradient variance is lowest and MAPPO and IPPO have the best chance of producing meaningful learning progress.

Learning Curves. Figure 3 compares training dynamics at $N \in \{2, 5, 10\}$. At $N=2$, DG-PG converges to near-Best-Fit performance within 5 episodes and remains stable, while MAPPO and IPPO briefly approach similar levels but subsequently deteriorate. At $N=5$, the advantage becomes more pronounced, with DG-PG achieving a mean reward of -14.2 (close to Best-Fit’s -12.6), while MAPPO (-34.1) and IPPO (-39.8) plateau at $2\text{--}3\times$ worse performance. At $N=10$, IPPO deteriorates sharply (-49.3), confirming that independent learning fails as coordination demands grow. In contrast, DG-PG reaches -11.7 , *surpassing* the Best-Fit heuristic through temporal strategies unavailable to the single-step greedy policy. These results confirm that gradient guidance is the decisive factor; the natural next question is whether this advantage persists at larger scales.

6.4. Scalability

We next evaluate DG-PG at scales from $N=5$ to $N=200$, comparing against heuristic baselines on 40 held-out test scenarios. MAPPO and IPPO are excluded as they fail to converge at any tested scale despite extensive tuning (Appendix J).

Best Checkpoint Performance. Figure 4 and Table 1 summarize best checkpoint performance (mean \pm std over 40 test scenarios). DG-PG matches or exceeds the Best-Fit heuristic at scales $N \leq 100$, demonstrating that the learned

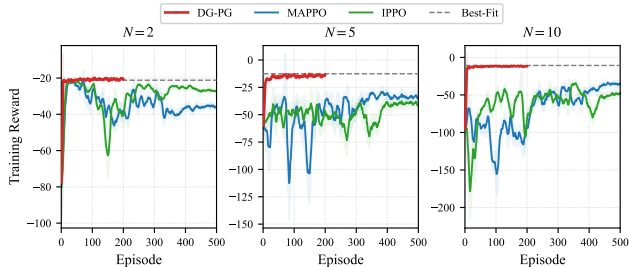


Figure 3. **Controlled comparison.** Training reward for $N \in \{2, 5, 10\}$. DG-PG (200 episodes, red) converges rapidly to the Best-Fit reference (dashed). MAPPO and IPPO (500 episodes) remain far below despite $2.5\times$ more training.

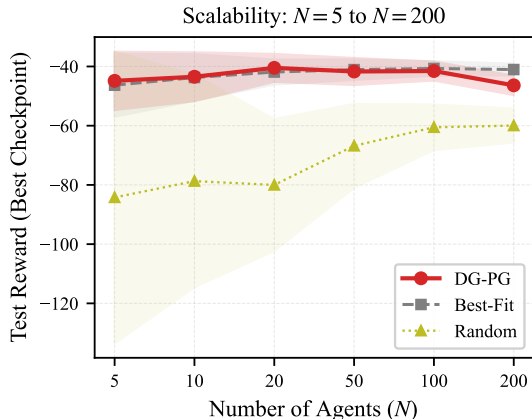


Figure 4. **Scalability.** Best checkpoint test reward vs. number of agents N . DG-PG closely tracks the Best-Fit heuristic across all scales, while Random degrades with N .

policy captures coordination strategies beyond the greedy single-step assignment. At $N=200$, a modest gap emerges (-46.4 vs. -41.0), which we attribute to the growing gradient variance at large N ; scale-adaptive α scheduling is a promising direction to close this gap.

Scale-Invariant Convergence. Figure 5 overlays DG-PG’s training curves across all scales. Notably, DG-PG converges to within 10% of its best observed reward in ≤ 10 episodes at *every* scale, from $N=5$ to $N=200$. The near-perfect alignment of the six curves provides direct empirical confirmation of the agent-independent sample complexity predicted by Theorem 4.3: the number of episodes required for convergence *does not grow with* N .

Computational Cost. The rapid convergence (≤ 10 episodes) translates to practical training times even on consumer hardware. On a single laptop CPU (Apple M1, no GPU), DG-PG converges within ~ 1 minute at $N=5$, ~ 3 minutes at $N=20$, and ~ 35 minutes at $N=200$. Complete training (200 episodes) takes ~ 12 hours at the largest scale. Detailed per-scale timing and breakdown are provided in Appendix K.

Table 1. Best checkpoint reward on 40 test scenarios (mean \pm std). MAPPO and IPPO fail to converge at any scale and are excluded.

	$N=5$	$N=10$	$N=20$	$N=50$	$N=100$	$N=200$
DG-PG (ours)	-44.9 ± 9.8	-43.5 ± 8.2	-40.5 ± 4.7	-41.7 ± 4.5	-41.5 ± 3.2	-46.4 ± 3.3
Best-Fit	-46.3 ± 10.7	-43.7 ± 7.8	-41.9 ± 4.2	-41.1 ± 3.4	-40.7 ± 2.4	-41.0 ± 1.9
Random	-84.2 ± 49.2	-78.7 ± 35.8	-80.0 ± 22.2	-66.8 ± 14.1	-60.5 ± 7.7	-60.0 ± 5.7

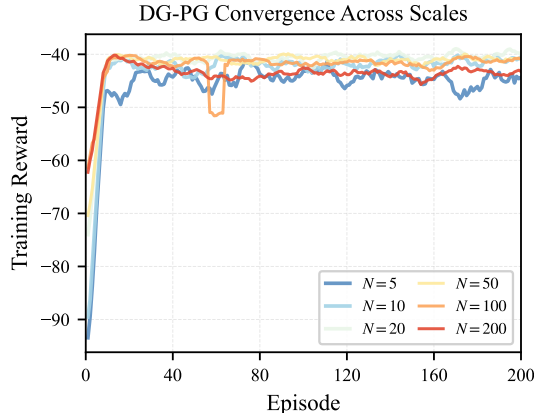


Figure 5. **Scale-invariant convergence.** DG-PG training reward across $N \in \{5, 10, 20, 50, 100, 200\}$. All scales converge within ~ 10 episodes, empirically confirming $\mathcal{O}(1)$ sample complexity.

DG-PG’s rapid convergence produces policies that generalize well beyond training. Performance remains stable as α decays from 0.9 to 0.2, indicating that agents internalize effective coordination patterns early and do not depend on the guidance signal to maintain them. Unlike residual policy methods, which require the base controller to remain online at deployment, DG-PG uses the analytical reference only during training. At test time, the policy runs independently without guidance. On 40 held-out test scenarios, where the guidance signal is entirely absent, the resulting decentralized policy matches or exceeds Best-Fit, a centralized heuristic with access to full global state, across the majority of tested scales (Table 1).

7. Conclusion

In this work, we identified cross-agent noise as the central bottleneck in scaling cooperative MARL. DG-PG addresses this by augmenting each agent’s policy gradient with an analytically computed per-agent guidance term derived from a domain-specific reference model. This reduces gradient variance from $\Theta(N)$ to $\mathcal{O}(1)$ while preserving the Nash equilibria of the original game. Experiments on a heterogeneous cloud scheduling benchmark confirm that DG-PG maintains consistent performance from 5 to 200 agents, while standard multi-agent policy gradient methods degrade rapidly with N .

DG-PG requires only that the analytical model indicate a beneficial direction for the system state, not that the refer-

ence be exactly achievable or directly translatable into agent actions. This makes DG-PG applicable to any cooperative domain where approximate analytical models are available, such as traffic networks and supply chains.

Limitations and future work. DG-PG is applicable to cooperative domains where an analytical model with informative gradients is available, and problems without such structure need alternative approaches. The guidance weight α follows a fixed schedule independent of N . Scale-adaptive scheduling that increases guidance at larger N is a promising direction to close the remaining gap at $N=200$.

References

- Agarwal, A., Kakade, S. M., Lee, J. D., and Mahajan, G. On the theory of policy gradient methods: Optimality, approximation, and distribution shift. *Journal of Machine Learning Research*, 22(98):1–76, 2021.
- Bertsekas, D. and Gallager, R. *Data networks*. Athena Scientific, 2021.
- Cortez, E., Bonde, A., Muzio, A., Russinovich, M., Fontoura, M., and Bianchini, R. Resource central: Understanding and predicting workloads for improved resource management in large cloud platforms. In *Proceedings of the 26th Symposium on Operating Systems Principles*, pp. 153–167, 2017.
- Delimitrou, C. and Kozyrakis, C. Quasar: Resource-efficient and QoS-aware cluster management. In *Proceedings of the 19th International Conference on Architectural Support for Programming Languages and Operating Systems (ASPLOS)*, pp. 127–144, 2014.
- El-Tantawy, S., Abdulhai, B., and Abdelgawad, H. Multi-agent reinforcement learning for integrated network of adaptive traffic signal controllers (marlin-atssc): Methodology and large-scale application on downtown toronto. *IEEE transactions on Intelligent transportation systems*, 14(3):1140–1150, 2013.
- Foerster, J., Farquhar, G., Afouras, T., Nardelli, N., and Whiteson, S. Counterfactual multi-agent policy gradients. In *Proceedings of the AAAI conference on artificial intelligence*, volume 32, 2018.
- Ghods, A., Zaharia, M., Hindman, B., Konwinski, A., Shenker, S., and Stoica, I. Dominant resource fairness: Fair allocation of multiple resource types. In *8th USENIX symposium on networked systems design and implementation (NSDI 11)*, 2011.
- Johannink, T., Bahl, S., Nair, A., Luo, J., Kumar, A., Loskyll, M., Ojea, J. A., Solowjow, E., and Levine, S. Residual reinforcement learning for robot control. In *2019 international conference on robotics and automation (ICRA)*, pp. 6023–6029. IEEE, 2019.
- Karimi, H., Nutini, J., and Schmidt, M. Linear convergence of gradient and proximal-gradient methods under the polyak-łojasiewicz condition. In *Joint European conference on machine learning and knowledge discovery in databases*, pp. 795–811. Springer, 2016.
- Kelly, F. P., Maulloo, A. K., and Tan, D. K. H. Rate control for communication networks: shadow prices, proportional fairness and stability. *Journal of the Operational Research society*, 49(3):237–252, 1998.
- Kuba, J. G., Wen, M., Meng, L., Zhang, H., Mguni, D., Wang, J., and Yang, Y. Settling the variance of multi-agent policy gradients. *Advances in Neural Information Processing Systems*, 34:13458–13470, 2021.
- Kuba, J. G., Chen, R., Wen, M., Wen, Y., Sun, F., Wang, J., and Yang, Y. Trust region policy optimisation in multi-agent reinforcement learning. In *International Conference on Learning Representations*, 2022.
- Kurtz, T. G. *Approximation of population processes*. SIAM, 1981.
- Levine, S. and Koltun, V. Guided policy search. In *International conference on machine learning*, pp. 1–9. PMLR, 2013.
- Mao, H., Schwarzkopf, M., Venkatakrisnan, S. B., Meng, Z., and Alizadeh, M. Learning scheduling algorithms for data processing clusters. In *Proceedings of the ACM Special Interest Group on Data Communication (SIGCOMM)*, pp. 270–288, 2019.
- Mei, J., Xiao, C., Szepesvari, C., and Schuurmans, D. On the global convergence rates of softmax policy gradient methods. In *International Conference on Machine Learning*, pp. 6820–6829. PMLR, 2020.
- Ng, A. Y., Harada, D., and Russell, S. Policy invariance under reward transformations: Theory and application to reward shaping. In *International Conference on Machine Learning*, pp. 278–287, 1999.
- Oliehoek, F. A. and Amato, C. *A concise introduction to decentralized POMDPs*. Springer, 2016.
- Raissi, M., Perdikaris, P., and Karniadakis, G. E. Physics-informed neural networks: A deep learning framework for solving forward and inverse problems involving nonlinear partial differential equations. *Journal of Computational physics*, 378:686–707, 2019.
- Rashid, T., Samvelyan, M., De Witt, C. S., Farquhar, G., Foerster, J., and Whiteson, S. Monotonic value function

- factorisation for deep multi-agent reinforcement learning. *Journal of Machine Learning Research*, 21(178):1–51, 2020.
- Reiss, C., Wilkes, J., and Hellerstein, J. L. Google cluster-usage traces: format+ schema. *Google Inc., White Paper*, 1:1–14, 2011.
- Reiss, C., Tumanov, A., Ganger, G. R., Katz, R. H., and Kozuch, M. A. Heterogeneity and dynamicity of clouds at scale: Google trace analysis. In *Proceedings of the third ACM symposium on cloud computing*, pp. 1–13, 2012.
- Schulman, J., Moritz, P., Levine, S., Jordan, M. I., and Abbeel, P. High-dimensional continuous control using generalized advantage estimation. In *International Conference on Learning Representations*, 2016.
- Sunehag, P., Lever, G., Gruslys, A., Czarnecki, W. M., Zambaldi, V., Jaderberg, M., Lanctot, M., Sonnerat, N., Leibo, J. Z., Tuyls, K., et al. Value-decomposition networks for cooperative multi-agent learning. *arXiv preprint arXiv:1706.05296*, 2017.
- Sutton, R. S. and Barto, A. G. *Reinforcement learning: An introduction*. MIT press Cambridge, 1998.
- Sutton, R. S., McAllester, D., Singh, S., and Mansour, Y. Policy gradient methods for reinforcement learning with function approximation. *Advances in neural information processing systems*, 12, 1999.
- Wang, J., Ren, Z., Liu, T., Yu, Y., and Zhang, C. Qplex: Duplex dueling multi-agent q-learning. In *International Conference on Learning Representations*, 2021.
- Wardrop, J. G. Road paper. some theoretical aspects of road traffic research. *Proceedings of the institution of civil engineers*, 1(3):325–362, 1952.
- Wolpert, D. H. and Tumer, K. Optimal payoff functions for members of collectives. *Advances in Complex Systems*, 4 (02n03):265–279, 2001.
- Wood, A. J., Wollenberg, B. F., and Sheblé, G. B. *Power generation, operation, and control*. John wiley & sons, 2013.
- Yang, Y., Luo, R., Li, M., Zhou, M., Zhang, W., and Wang, J. Mean field multi-agent reinforcement learning. In *International conference on machine learning*, pp. 5571–5580. PMLR, 2018.
- Yu, C., Velu, A., Vinitsky, E., Gao, J., Wang, Y., Bayen, A., and Wu, Y. The surprising effectiveness of ppo in cooperative multi-agent games. *Advances in neural information processing systems*, 35:24611–24624, 2022.

A. Comparison with Existing Methods

Table 2 provides a systematic comparison of DG-PG with representative methods from major paradigms in cooperative MARL. We evaluate methods across key dimensions, including gradient variance scaling, sample complexity, support for heterogeneous policies, parallel updates, architectural overhead, and domain knowledge requirements. The comparison highlights DG-PG’s unique position as the only method that simultaneously achieves $\mathcal{O}(1)$ gradient variance, supports heterogeneous agent policies with parallel updates, and requires no additional learned components beyond a standard centralized critic.

Table 2. Systematic comparison of cooperative MARL methods across key architectural and algorithmic dimensions. DG-PG is the only method that simultaneously achieves $\mathcal{O}(1)$ variance, $\mathcal{O}(1/\epsilon)$ sample complexity, full heterogeneity support, parallel updates, and zero extra learned components.

Method	Approach	Variance Scaling	Sample Complexity	Heterog. Policies	Parallel Updates	Extra Learned Components	Assumption / Requirement
<i>Policy Gradient Methods</i>							
MAPPO (Yu et al., 2022)	Centralized PG	$\Theta(N)$	$\mathcal{O}(N/\epsilon)$	✓	✓	None	None
IPPO (Yu et al., 2022)	Independent PG	$\Theta(N)$	$\mathcal{O}(N/\epsilon)$	✓	✓	None	None
HAPPO (Kuba et al., 2022)	Sequential PG	$\mathcal{O}(1)^\dagger$	$\mathcal{O}(N/\epsilon)^\dagger$	✓	×	None	None
COMA (Foerster et al., 2018)	Counterfactual	$\Theta(N)^\ddagger$	$\mathcal{O}(N/\epsilon)$	✓	✓	N critic heads	None
<i>Value Decomposition Methods</i>							
QMIX (Rashid et al., 2020)	Mixing Network	N/A (Value)	—	✓	✓	Mixing net	Monotonicity
VDN (Sunehag et al., 2017)	Additive	N/A (Value)	—	✓	✓	None	Additivity
QPLEX (Wang et al., 2021)	Attention	N/A (Value)	—	✓	✓	Attn mixer, $\mathcal{O}(N^2)$	Dueling struct.
<i>Mean-Field Approximation</i>							
Mean-Field (Yang et al., 2018)	Neighbor Avg.	$\mathcal{O}(1)^\S$	$\mathcal{O}(1/\epsilon)^\S$	×	✓	None	Exchangeability
<i>Reward Modification Methods</i>							
PBRS (Ng et al., 1999)	Potential Shaping	$\Theta(N)$	$\mathcal{O}(N/\epsilon)$	✓	✓	None	Potential func.
Diff. Rewards (Wolpert & Tumer, 2001)	Counterfactual	Problem-dep.*	Problem-dep.*	✓	✓	None	Exact simulator
<i>Gradient Guidance (Proposed)</i>							
DG-PG (Ours)	Analytic Guide	$\mathcal{O}(1)$	$\mathcal{O}(1/\epsilon)$	✓	✓	None	Analytical model

Notes: “Variance Scaling” = per-agent gradient variance w.r.t. N ; “Sample Complexity” = number of iterations to reach ϵ -optimality (proven bounds for PG methods); “Extra Learned Components” = trainable modules beyond standard actor-critic; “—” = not directly comparable (value-based methods lack explicit PG complexity bounds).

[†]HAPPO reduces per-agent variance via sequential updates with trust-region constraints, but sacrifices parallelism. Consequently, wall-clock time per iteration scales as $\mathcal{O}(N)$, yielding effective sample complexity $\mathcal{O}(N/\epsilon)$ in wall-clock time.

[‡]COMA requires N separate critic heads to compute counterfactual baselines. Reduces own-action variance σ_{self}^2 but does not suppress cross-agent noise $(N - 1)\sigma_{\text{others}}^2$.

*Difference Rewards reduce variance by subtracting a counterfactual baseline $r(s, \mathbf{a}) - r(s, \mathbf{a}^{-i})$, but the degree of reduction depends on the reward structure (separability). For non-separable rewards, cross-agent interaction terms persist. Computing the counterfactual also requires an exact simulator, which is often intractable at scale.

[§]Mean-Field methods assume homogeneous agents (identical and exchangeable). Results hold only under this approximation, and convergence is to the mean-field equilibrium, which may differ from the Nash equilibrium of the original N -agent game.

Key Insights from the Comparison

1. Every existing method sacrifices at least one critical property. For large-scale cooperative MARL, we identify five desirable properties: $\mathcal{O}(1)$ variance, $\mathcal{O}(1/\epsilon)$ sample complexity, heterogeneous policies, parallel updates, and zero extra learned components. No prior method achieves all five:

- **MAPPO / IPPO:** $\Theta(N)$ variance \Rightarrow $\mathcal{O}(N/\epsilon)$ sample complexity.
- **HAPPO:** sequential updates \Rightarrow $\mathcal{O}(N)$ wall-clock cost per iteration.
- **Mean-Field:** requires agent exchangeability \Rightarrow no heterogeneous policies.
- **QMIX / QPLEX:** extra mixing networks or $\mathcal{O}(N^2)$ attention layers.
- **Diff. Rewards:** requires an exact simulator, often intractable at scale.

DG-PG satisfies all five simultaneously (Theorems 4.2–4.3), with only a minimal modification to the advantage computation in standard policy gradient algorithm such as MAPPO.

2. Leveraging analytical models without sacrificing optimality. All other methods in Table 2 are purely model-free, either imposing no assumptions at all (MAPPO, IPPO, HAPPO, COMA) or encoding structural constraints into the architecture (QMIX, VDN, Mean-Field). DG-PG is unique in leveraging an *external analytical model* to reduce variance while remaining model-free in its convergence guarantees.

DG-PG’s gradient-level use of analytical models also distinguishes it from other knowledge-informed learning paradigms: Physics-Informed Neural Networks (Raissi et al., 2019) embed governing equations directly into the loss, requiring exact PDEs; Residual RL (Johannink et al., 2019) uses a hand-designed controller as a permanent base policy, inheriting its biases; Guided Policy Search (Levine & Koltun, 2013) relies on trajectory optimization with known dynamics. These methods all incorporate domain knowledge into the objective or policy. In contrast, DG-PG derives the gradient of a guidance term from the analytical model to steer policy updates, leaving the original objective J unchanged. As a result, model inaccuracies affect only variance, not the Nash equilibria of the original game (Theorem 4.1). The adjustable α further allows practitioners to tune the degree of reliance based on model fidelity.

B. Theoretical Assumptions and Dependencies

For reviewer convenience, Table 3 summarizes the dependency structure between our theoretical results and the assumptions they rely upon.

Table 3. Dependency of theoretical results on assumptions. “✓” indicates that the result requires the corresponding assumption. All assumptions are stated in the main text (Section 3.1) and Appendix G.

Result	Exogeneity (Asm. 3.1)	Alignment (Asm. 3.2)	Smoothness & PL (Asm. G.1)	Bounded Variance	Role of Assumptions
Thm. 4.1 (Nash Invariance)	✓	✓			Exogeneity ensures reference does not shift; Alignment ensures guidance gradient vanishes at Nash equilibria.
Thm. 4.2 (Variance Bound)	✓	✓			Exogeneity makes reference deterministic; Alignment ensures negative correlation $\rho < 0$.
Thm. 4.3 (Sample Complexity)	✓	✓	✓	✓	Smoothness enables the per-iteration bound; PL condition yields linear convergence rate; $\mathcal{O}(1)$ variance from Thm. 4.2.
Prop. 1 in App. C.3 (Cloud Verification)					Standalone verification that Alignment holds for cloud scheduling via Cauchy-Schwarz on the load imbalance functional.

Discussion of Assumption Strength.

- **Assumption 3.1 (Exogeneity)** is a design choice rather than a restrictive condition. It is satisfied by construction when the reference is computed from exogenous system parameters (e.g., server capacities, total workload) and treated as a fixed target during gradient computation via the stop-gradient operator $\perp(\cdot)$.
- **Assumption 3.2 (Descent-Aligned Reference)** is the core structural requirement. It holds when the analytical model captures the dominant performance drivers of the cooperative objective. We verify this rigorously for cloud scheduling in Appendix C.3 and outline verification templates for traffic, communication, and power grid domains.
- **Assumption G.1 (Smoothness & PL)** is standard in the stochastic optimization literature and is required only for the convergence rate result (Theorem 4.3). The variance reduction (Theorem 4.2) and Nash invariance (Theorem 4.1) hold without these regularity conditions.

C. Case Study: Verification of Structural Assumptions

In this appendix, we provide a detailed verification that the structural Assumptions 3.1 and 3.2 hold for the cloud resource scheduling task used in our experiments. This serves as a representative case study demonstrating how domain-specific

priors can be systematically validated within the DG-PG framework.

Applicability to Other Domains. While we focus on cloud scheduling, similar verification procedures apply to other control problems where analytical priors are available:

- *Communication networks:* Network utility maximization theory provides proportional fairness as a natural reference allocation (Kelly et al., 1998).
- *Power grids:* DC optimal power flow and economic dispatch yield reference generation schedules (Wood et al., 2013).
- *Traffic systems:* Wardrop equilibrium and system-optimal routing define reference flow distributions (Wardrop, 1952).

In each case, the key requirement is that the prior defines a descent direction aligned with the cooperative objective, a property we formally verify below for the cloud scheduling domain using fluid-limit analysis from queueing theory (Kurtz, 1981).

C.1. System Model and Objective Approximation

System Setup. We study a cooperative multi-agent system for task scheduling in a heterogeneous cluster of N servers. Tasks are characterized by multi-dimensional resource requirements (e.g., CPU, memory), and servers possess heterogeneous capacities across these dimensions. Let K denote the number of resource types. We model the system state using the full resource utilization vector.

Specifically, let $\mathbf{x}_t^i = (x_t^{i,1}, \dots, x_t^{i,K})^\top \in \mathbb{R}_{\geq 0}^K$ denote the *resource utilization vector* on server i at time t , where $x_t^{i,k}$ is the load on the k -th resource dimension. The server capacities are given by $\boldsymbol{\mu}^i = (\mu^{i,1}, \dots, \mu^{i,K})^\top$, where $\mu^{i,k}$ is the maximum processing rate of server i on resource dimension k . This generalization captures the coupling between resources, avoiding the information loss associated with scalar bottleneck abstractions.

The total workload pressure in the system on dimension k , denoted as C^k , is conserved under task assignment decisions:

$$\sum_{i=1}^N x_t^{i,k} = C^k, \quad x_t^{i,k} \geq 0, \quad \forall t, \forall k.$$

Surrogate Objective via Queueing Theory. To construct the reference state $\tilde{\mathbf{X}}$, we need an analytically tractable objective whose minimizer serves as the guidance target. The cooperative MARL objective J itself is intractable because it aggregates queueing delay, energy efficiency, and fairness through complex, non-separable interactions. However, queueing theory reveals that improving each of these criteria reduces to a common structural condition:

- **Queueing delay** is a convex function of server utilization, scaling as $1/(\mu - x)$ near capacity (Bertsekas & Gallager, 2021). By Jensen’s inequality, total delay is minimized when utilization is equalized across servers.
- **Energy cost** in heterogeneous clusters with varying $\mu^{i,k}$ is minimized by capacity-proportional allocation, which avoids overloading low-efficiency machines.
- **Fairness** improves as utilization variance decreases, reducing service-level violations on congested servers.

All three criteria improve when server utilization is balanced proportionally to capacity. We formalize this shared structure as the *load imbalance functional*:

$$\mathcal{J}_{\text{load}}(\mathbf{X}) \triangleq \sum_{k=1}^K \sum_{i=1}^N \frac{1}{\mu^{i,k}} (x^{i,k})^2, \tag{18}$$

where $\mathbf{X} = \{\mathbf{x}^1, \dots, \mathbf{x}^N\}$ is the global system state. The gradient $\frac{\partial \mathcal{J}_{\text{load}}}{\partial x^{i,k}} = \frac{2x^{i,k}}{\mu^{i,k}}$ is proportional to the utilization rate of resource k on server i , so minimizing $\mathcal{J}_{\text{load}}$ drives the system toward capacity-proportional allocation. Crucially, $\mathcal{J}_{\text{load}}$ is convex and separable across resource dimensions, admitting a closed-form minimizer. This tractability also enables rigorous verification of Assumption 3.2, which would be intractable for the composite objective J directly.

Optimal Reference via Load Balancing. To construct the reference state $\tilde{\mathbf{X}}$, we solve the constrained optimization problem of minimizing $\mathcal{J}_{\text{load}}$ under workload conservation. For each resource dimension k , this reduces to:

$$\min_{\mathbf{X}} \sum_{i=1}^N \frac{1}{\mu^{i,k}} (x^{i,k})^2 \quad \text{subject to} \quad \sum_{i=1}^N x^{i,k} = C^k.$$

This is a classical convex optimization problem whose solution is well-established in queueing theory and resource allocation (Bertsekas & Gallager, 2021; Ghodsi et al., 2011). Constructing the Lagrangian for dimension k :

$$\mathcal{L}_{\text{Lag}}^k(\mathbf{x}^{\cdot,k}, \lambda_k) = \sum_{i=1}^N \frac{1}{\mu^{i,k}} (x^{i,k})^2 - \lambda_k \left(\sum_{i=1}^N x^{i,k} - C^k \right),$$

and taking the first-order optimality condition:

$$\frac{\partial \mathcal{L}_{\text{Lag}}^k}{\partial x^{i,k}} = \frac{2x^{i,k}}{\mu^{i,k}} - \lambda_k = 0 \quad \implies \quad x^{i,k} = \frac{\lambda_k \mu^{i,k}}{2}.$$

This shows that at the optimum, load is allocated proportionally to capacity: $x^{i,k} \propto \mu^{i,k}$. Applying the workload constraint $\sum_i x^{i,k} = C^k$ yields:

$$x^{*,i,k} = \frac{\mu^{i,k}}{\sum_j \mu^{j,k}} \cdot C^k.$$

Equivalently, the optimal state satisfies the *utilization balancing condition*, i.e., the utilization rate $x^{i,k}/\mu^{i,k}$ is equalized across all servers for each resource type k :

$$\frac{x^{1,k}}{\mu^{1,k}} = \frac{x^{2,k}}{\mu^{2,k}} = \dots = \frac{x^{N,k}}{\mu^{N,k}}, \quad \forall k \in \{1, \dots, K\}.$$

This principle is fundamental to heterogeneous resource allocation and aligns with dominant resource fairness (DRF) in multi-dimensional scheduling systems.

Theory-Guided Reference State. Based on the optimal solution derived above, we define the *capacity-weighted load-balancing equilibrium* as our theory-guided reference:

$$\tilde{x}_t^{i,k} = \frac{\mu^{i,k}}{\sum_{j=1}^N \mu^{j,k}} \cdot C^k, \quad \forall i, k. \quad (19)$$

By construction, $\tilde{\mathbf{X}}_t = \{\tilde{x}_t^1, \dots, \tilde{x}_t^N\}$ is the unique global minimizer of $\mathcal{J}_{\text{load}}(\mathbf{X})$ under the workload constraints. Note that $\tilde{\mathbf{X}}_t$ is derived from a continuous (fluid) optimization and may not be exactly reachable under discrete task assignments; however, this does not affect the verification below. We now verify that this reference satisfies Assumptions 3.1 and 3.2; specifically, in Appendix C.3, we prove that $(\tilde{\mathbf{X}} - \mathbf{X})$ is aligned with the descent direction of $\mathcal{J}_{\text{load}}$, guaranteeing that moving toward the reference reduces load imbalance.

C.2. Verification of Assumption 3.1 (Exogeneity)

The reference state $\tilde{\mathbf{X}}_t$ is computed deterministically from the current aggregate system workload C^k but is treated as a fixed constant during the policy gradient computation step. Specifically, for each server i and resource k , we define:

$$\tilde{x}_t^{i,k} := \perp \left(\frac{\mu^{i,k}}{\sum_{j=1}^N \mu^{j,k}} \cdot C^k \right).$$

Here, \perp denotes the stop-gradient operator. Since $\tilde{\mathbf{X}}_t$ depends only on the current state information (total load) and not on the immediate action a_t selected by the policy π_θ , we have $\nabla_\theta \tilde{\mathbf{X}}_t = \mathbf{0}$, ensuring that no gradient flows back through the reference target. This satisfies Assumption 3.1.

C.3. Verification of Assumption 3.2 (Directional Alignment)

Assumption 3.2 requires that the direction $(\tilde{\mathbf{X}} - \mathbf{X})$ is a descent direction for the cooperative objective J . Since $\mathcal{J}_{\text{load}}$ is a surrogate for J justified by queueing theory (Section C), it suffices to show that $(\tilde{\mathbf{X}} - \mathbf{X})$ is a descent direction for $\mathcal{J}_{\text{load}}$.

Proposition C.1 (Alignment with Load Imbalance Reduction). *For any feasible state $\mathbf{X} \neq \tilde{\mathbf{X}}$ satisfying the workload constraints, the direction $(\tilde{\mathbf{X}} - \mathbf{X})$ is aligned with the descent direction of the load imbalance functional:*

$$\langle \nabla_{\mathbf{X}} \mathcal{J}_{\text{load}}(\mathbf{X}), \tilde{\mathbf{X}} - \mathbf{X} \rangle < 0.$$

That is, moving towards $\tilde{\mathbf{X}}$ reduces load imbalance.

Proof. Using the definition of the load imbalance functional in Equation 18, we compute the inner product between its gradient and the guidance vector. Since $\mathcal{J}_{\text{load}}$ is separable across resource dimensions, the total inner product decomposes as a sum over resource types k :

$$\begin{aligned} \langle \nabla_{\mathbf{X}} \mathcal{J}_{\text{load}}, \tilde{\mathbf{X}} - \mathbf{X} \rangle &= \sum_{k=1}^K \sum_{i=1}^N \frac{\partial \mathcal{J}_{\text{load}}}{\partial x^{i,k}} (\tilde{x}^{i,k} - x^{i,k}) \\ &= \sum_{k=1}^K \underbrace{\sum_{i=1}^N \frac{2x^{i,k}}{\mu^{i,k}} (\tilde{x}^{i,k} - x^{i,k})}_{I_k}. \end{aligned}$$

To establish that the total inner product is negative, it suffices to show that each component $I_k \leq 0$. We analyze a fixed resource dimension k . First, observe that by the equilibrium definition in Equation 19, the reference utilization rate is constant across all servers:

$$\frac{\tilde{x}^{i,k}}{\mu^{i,k}} = \frac{C^k}{\sum_{j=1}^N \mu^{j,k}}.$$

Substituting this constant ratio into the expression for I_k :

$$\begin{aligned} I_k &= 2 \sum_{i=1}^N x^{i,k} \left(\frac{\tilde{x}^{i,k}}{\mu_i^k} - \frac{x^{i,k}}{\mu_i^k} \right) \\ &= 2 \left(\frac{C^k}{\sum_{j=1}^N \mu_j^k} \right) \sum_{i=1}^N x^{i,k} - 2 \sum_{i=1}^N \frac{(x^{i,k})^2}{\mu^{i,k}} \\ &= \frac{2(C^k)^2}{\sum_{j=1}^N \mu^{j,k}} - 2 \sum_{i=1}^N \frac{(x^{i,k})^2}{\mu^{i,k}}. \end{aligned}$$

To determine the sign of I_k , we apply the Cauchy-Schwarz inequality to vectors $\mathbf{u} = \left(\frac{x^{i,k}}{\sqrt{\mu^{i,k}}} \right)_i$ and $\mathbf{v} = \left(\sqrt{\mu^{i,k}} \right)_i$:

$$\left(\sum_{i=1}^N u_i v_i \right)^2 \leq \left(\sum_{i=1}^N u_i^2 \right) \left(\sum_{i=1}^N v_i^2 \right).$$

Substituting the definitions of u_i and v_i :

$$\left(\sum_{i=1}^N x^{i,k} \right)^2 \leq \left(\sum_{i=1}^N \frac{(x^{i,k})^2}{\mu^{i,k}} \right) \left(\sum_{i=1}^N \mu^{i,k} \right).$$

Rearranging terms and using $\sum x^{i,k} = C^k$:

$$\sum_{i=1}^N \frac{(x^{i,k})^2}{\mu^{i,k}} \geq \frac{(C^k)^2}{\sum_{j=1}^N \mu^{j,k}}.$$

Comparing this with the expression for I_k , we see that the second term (actual variance) is always greater than or equal to the first term (minimal variance). Thus, $I_k \leq 0$ for all k , with strict inequality if the system is unbalanced. Summing over all dimensions implies:

$$\langle \nabla_{\mathbf{X}} \mathcal{J}_{\text{load}}(\mathbf{X}), \tilde{\mathbf{X}} - \mathbf{X} \rangle = \sum_{k=1}^K I_k < 0.$$

This confirms that the direction toward the reference $\tilde{\mathbf{X}}$ is *aligned with the descent direction* of the load imbalance functional, thereby verifying Assumption 3.2. \square

Generalization to Other Domains. The verification procedure demonstrated above serves as a *template* for applying DG-PG to other systems. As outlined in the main text, domains such as communication networks (proportional fairness), power grids (economic dispatch), and traffic systems (Wardrop equilibrium) all admit analytical priors with similar structural properties. In each case, the key steps are: (1) identify a domain-specific performance metric with known convexity properties; (2) derive the reference state as its constrained optimum; (3) verify that the reference defines a descent direction using tools from convex analysis or variational inequalities. This case study establishes the feasibility and rigor of such verification, providing a blueprint for extending DG-PG beyond cloud scheduling.

Robustness to Approximate Satisfaction. In practice, the structural assumptions may not hold exactly. For instance, the fluid-limit approximation underlying the reference state assumes Poisson arrivals and homogeneous service times, which are often violated in real systems due to heavy-tailed workloads and temporal fluctuations. However, DG-PG remains effective as long as the assumptions hold *approximately*, that is, the reference captures the dominant performance drivers even if the analytical model is idealized. The adjustable guidance weight α provides a natural mechanism for handling model inaccuracies. When the prior is less accurate, reducing α diminishes its influence while preserving the variance reduction benefits. Our experiments (Section 6.2) demonstrate that DG-PG is robust across a range of α values, confirming that directional correctness, rather than exact model fidelity, is sufficient for effective guidance.

D. Derivation of Local Influence Vector

In this appendix, we derive the local influence vector $\mathbf{z}_t^i = \frac{\partial \mathbf{x}_t}{\partial a_t^i}$ for the cloud resource scheduling example. Here \mathbf{z}_t^i captures the marginal effect of agent i 's action on the system state, i.e., how choosing a particular server changes the global utilization vector. This derivation generalizes to other domains with similar additive structure.

We use the notation established in Appendix C: N servers, K resource dimensions, global utilization vector $\mathbf{x}_t \in \mathbb{R}^{NK}$, and per-server utilization $\mathbf{x}_t^j \in \mathbb{R}^K$. Each agent i holds a task with resource requirement vector $\mathbf{w}^i = (w^{i,1}, \dots, w^{i,K})^\top \in \mathbb{R}^K$, where $w^{i,k}$ is the demand on resource dimension k (e.g., CPU cores, memory). Each agent i selects a target server $a_t^i \in \{1, \dots, N\}$, and the next-step utilization on server j is determined by the joint actions of all agents:

$$\mathbf{x}_{t+1}^j = \mathbf{x}_t^j + \sum_{l=1}^N \mathbf{w}^l \cdot \mathbb{I}(a_t^l = j).$$

To compute the marginal effect of agent i 's action, we differentiate with respect to a_t^i . Since the contributions of all other agents $l \neq i$ are held fixed, their terms vanish, leaving only agent i 's contribution:

$$\mathbf{z}_t^i \triangleq \frac{\partial \mathbf{x}_{t+1}}{\partial a_t^i} = (\mathbf{0}, \dots, \underbrace{\mathbf{w}^i}_{\text{server } j}, \dots, \mathbf{0})^\top.$$

That is, assigning task i to server j increases server j 's load by exactly \mathbf{w}^i across all resource types, while leaving all other servers unaffected.

Projected coefficient. In the DG-PG update (Equations 8–10), each agent's guidance signal is scaled by the inner product $\langle \mathbf{x}_t - \tilde{\mathbf{x}}_t, \mathbf{z}_t^i \rangle$, which measures how much agent i 's action contributes to the change in deviation from the reference. Substituting the influence vector \mathbf{z}_t^i yields:

$$\langle \mathbf{x}_t - \tilde{\mathbf{x}}_t, \mathbf{z}_t^i \rangle = \sum_{k=1}^K w^{i,k} \cdot (x_t^{j,k} - \tilde{x}_t^{j,k}).$$

Each term measures how overloaded server j is on resource k , weighted by the task's own demand $w^{i,k}$, so resource types that the task consumes most heavily dominate the signal. Importantly, this coefficient provides a *direction* for policy improvement, not a hard constraint that forces convergence to $\tilde{\mathbf{X}}$. The actual system trajectory is determined by the learned policy interacting with the environment.

D.1. General Applicability

The key requirement is that the influence vector \mathbf{z}_t^i captures the marginal effect of an action on the system state. This structure arises naturally in many multi-agent systems:

- **Traffic routing:** \mathbf{x}_t represents link flows and actions are path selections, so \mathbf{z}_t^i indicates which links are used.
- **Inventory management:** \mathbf{x}_t represents stock levels and actions are replenishment orders, where \mathbf{z}_t^i adds to specific stock dimensions.
- **Communication networks:** \mathbf{x}_t represents channel interference levels and actions are power allocations, and \mathbf{z}_t^i captures each agent's marginal contribution to interference.

In each case, \mathbf{z}_t^i enables the projection-based variance reduction by isolating the relevant components of the global state deviation.

E. Detailed Proof of Nash Invariance (Theorem 4.1)

In this appendix, we provide the detailed proof for Theorem 4.1, establishing that our DG-PG framework preserves the Nash equilibria of the original cooperative game.

Theorem 4.1 (Nash Invariance). *Let θ^* be a Nash equilibrium of the original cooperative game, i.e., $\nabla_{\theta^i} J(\theta^*) = \mathbf{0}$ for all $i \in \mathcal{N}$. Under Assumptions 3.1–3.2, the DG-PG gradient also vanishes at θ^* , i.e., $\nabla_{\theta^i} J_\alpha(\theta^*) = \mathbf{0}$ for any $\alpha \in (0, 1)$ and all $i \in \mathcal{N}$.*

To prove this theorem, we first establish a key lemma stating that the gradient of the guidance term vanishes at any Nash equilibrium of the original game.

E.1. Lemma: Guidance Consistency

Lemma E.1. *Under Assumptions 3.1 and 3.2, if $\nabla_{\theta^i} J(\theta^*) = \mathbf{0}$ for all $i \in \mathcal{N}$, then $\nabla_{\theta^i} \mathcal{G}(\theta^*) = \mathbf{0}$ for all $i \in \mathcal{N}$.*

Proof. We proceed by contradiction. Suppose $\nabla_{\theta^i} J(\theta^*) = \mathbf{0}$ for all $i \in \mathcal{N}$ (the Nash condition), but $\nabla_{\theta^i} \mathcal{G}(\theta^*) \neq \mathbf{0}$ for some agent i . Recall that $\mathcal{G}(\theta) = \mathbb{E}_{s \sim \nu^\pi} [d(\mathbf{x}^\pi|_s, \tilde{\mathbf{x}}|_s)]$ is the expected deviation under the state visitation distribution ν^π , where $\mathbf{x}^\pi|_s$ is the system state jointly determined by agents' actions under policy π at MDP state s , and $\tilde{\mathbf{x}}|_s$ is the corresponding reference. We write $\mathbf{x}^* \triangleq \mathbf{x}^{\pi^*}|_s$ and $\tilde{\mathbf{x}} \triangleq \tilde{\mathbf{x}}|_s$ for a given MDP state s , where $\pi^* \triangleq \pi_{\theta^*}$.

Step 1. If $\mathbf{x}^* = \tilde{\mathbf{x}}$ for all states s visited under ν^{π^*} , then $d(\mathbf{x}^*, \tilde{\mathbf{x}}) = 0$ everywhere and $\mathcal{G}(\theta^*) = 0$. This is the global minimum of $\mathcal{G} \geq 0$, so the first-order condition gives $\nabla_{\theta^i} \mathcal{G}(\theta^*) = \mathbf{0}$ for all i , contradicting our assumption. Therefore there exists a visited state s at which $\mathbf{x}^* \neq \tilde{\mathbf{x}}$.

Step 2. By Assumption 3.2, at any state s where $\mathbf{x}^* \neq \tilde{\mathbf{x}}$:

$$\langle \nabla_{\mathbf{x}} J(\mathbf{x}^*), \tilde{\mathbf{x}} - \mathbf{x}^* \rangle > 0.$$

Since $\tilde{\mathbf{x}} - \mathbf{x}^* \neq \mathbf{0}$, the state-space gradient $\nabla_{\mathbf{x}} J(\mathbf{x}^*)$ must be non-zero.

Step 3. Under sufficient policy expressiveness (see Remark E.2), a non-zero state-space gradient $\nabla_{\mathbf{x}} J(\mathbf{x}^*) \neq \mathbf{0}$ implies $\nabla_{\theta^i} J(\theta^*) \neq \mathbf{0}$ for some agent i . This contradicts the Nash condition.

Therefore $\nabla_{\theta^i} \mathcal{G}(\theta^*) = \mathbf{0}$ for all $i \in \mathcal{N}$. □

Remark E.2 (Sufficient Expressiveness). The proof requires the Jacobian $\nabla_{\theta^i} \mathbf{x}$ to have full row rank for at least one agent i , ensuring that a non-zero state-space gradient $\nabla_{\mathbf{x}} J$ lifts to a non-zero parameter-space gradient $\nabla_{\theta^i} J$. This is a standard

condition for overparameterized neural network policies ($p \gg m$) and holds generically in the absence of degenerate symmetries.

E.2. Proof of Theorem 4.1

Proof. At a Nash equilibrium θ^* , we have $\nabla_{\theta^i} J(\theta^*) = \mathbf{0}$ for all $i \in \mathcal{N}$. By Lemma E.1, $\nabla_{\theta^i} \mathcal{G}(\theta^*) = \mathbf{0}$ for all $i \in \mathcal{N}$. Therefore:

$$\nabla_{\theta^i} J_\alpha(\theta^*) = (1 - \alpha)\nabla_{\theta^i} J(\theta^*) - \alpha\nabla_{\theta^i} \mathcal{G}(\theta^*) = \mathbf{0},$$

confirming that the augmentation does not alter the Nash equilibria of the original game. \square

F. Variance Decomposition and Reduction Analysis (Theorem 4.2)

In this appendix, we prove that the DG-PG estimator achieves agent-independent variance scaling. As established in Section 4.2, the standard policy gradient estimator has variance $\sigma_J^2 = \Theta(N)$ due to cross-agent exploration noise (Kuba et al., 2021), while the gradient estimator for the guidance term has variance $\sigma_G^2 = \mathcal{O}(1)$ since its coefficient depends only on deterministic quantities given a realized trajectory.

Theorem 4.2 (Agent-Independent Variance Bound). *Under Assumptions 3.1–3.2, let $\sigma_J^2 \triangleq \text{Var}(\hat{g}_J^i)$, $\sigma_G^2 \triangleq \text{Var}(\hat{g}_G^i)$, and $\rho \triangleq \text{Corr}(\hat{g}_J^i, \hat{g}_G^i) \in (-1, 0)$. The optimally weighted combined estimator achieves:*

$$\min_{\alpha \in (0,1)} \text{Var}(\hat{g}_{\text{DG}}^i) = \frac{\sigma_J^2 \sigma_G^2 (1 - \rho^2)}{\sigma_J^2 + \sigma_G^2 + 2\rho \sigma_J \sigma_G}.$$

Since $\sigma_J^2 = \Theta(N)$ and $\sigma_G^2 = \mathcal{O}(1)$, the minimum variance satisfies $\min_\alpha \text{Var}(\hat{g}_{\text{DG}}^i) = \mathcal{O}(1)$ for all N , independent of the number of agents.

F.1. Proof of Theorem 4.2

Proof. For the combined estimator $\hat{g}_{\text{DG}}^i = (1 - \alpha)\hat{g}_J^i - \alpha\hat{g}_G^i$, the variance is:

$$\sigma_{\text{DG}}^2(\alpha) = (1 - \alpha)^2 \sigma_J^2 + \alpha^2 \sigma_G^2 - 2\alpha(1 - \alpha)\rho \sigma_J \sigma_G, \quad (20)$$

where $\rho = \text{Corr}(\hat{g}_J^i, \hat{g}_G^i) \in (-1, 0)$ by Assumption 3.2.

The combined variance $\sigma_{\text{DG}}^2(\alpha)$ is a convex quadratic in α . To minimize it, we set $\frac{d}{d\alpha} \sigma_{\text{DG}}^2 = 0$:

$$-2(1 - \alpha)\sigma_J^2 + 2\alpha\sigma_G^2 - 2(1 - 2\alpha)\rho \sigma_J \sigma_G = 0 \implies \alpha^* = \frac{\sigma_J^2 + \rho \sigma_J \sigma_G}{\sigma_J^2 + \sigma_G^2 + 2\rho \sigma_J \sigma_G}. \quad (21)$$

Substituting α^* back into $\sigma_{\text{DG}}^2(\alpha)$, the minimum variance is:

$$\sigma_{\text{DG},\min}^2 = \frac{\sigma_J^2 \sigma_G^2 (1 - \rho^2)}{\sigma_J^2 + \sigma_G^2 + 2\rho \sigma_J \sigma_G}. \quad (22)$$

As established in Section 4.2, $\sigma_J^2 = \Theta(N)$ because the return aggregates all N agents' stochastic actions, while $\sigma_G^2 = \mathcal{O}(1)$ because the guidance coefficient is computed from deterministic quantities. Dividing numerator and denominator by σ_J^2 :

$$\sigma_{\text{DG},\min}^2 = \frac{\sigma_G^2 (1 - \rho^2)}{1 + \frac{\sigma_G^2}{\sigma_J^2} + 2\rho \frac{\sigma_G}{\sigma_J}} = \frac{\sigma_G^2 (1 - \rho^2)}{1 + \mathcal{O}(N^{-1})}.$$

The numerator $\sigma_G^2 (1 - \rho^2) = \mathcal{O}(1)$ since $\sigma_G^2 = \mathcal{O}(1)$ and $\rho \in (-1, 0)$ is a constant. The denominator $1 + \mathcal{O}(N^{-1})$ is bounded away from zero for all $N \geq 1$. Therefore:

$$\sigma_{\text{DG},\min}^2 = \mathcal{O}(1), \quad \text{for all } N \geq 1. \quad (23)$$

\square

Remark F.1. The optimal mixing coefficient $\alpha^* \rightarrow 1$ as $N \rightarrow \infty$, indicating that large-scale systems should rely primarily on the guidance signal to suppress cross-agent variance. In practice, we adopt a dynamic α schedule, starting with a large α for fast early convergence and decaying to a smaller value to allow the RL signal to fine-tune beyond the reference (see Section 6).

G. Convergence Rate and Sample Complexity (Theorem 4.3)

We establish the sample complexity of DG-PG under standard regularity conditions.

Theorem 4.3 (Sample Complexity). *Under the smoothness and PL conditions (Assumption G.1 below) and with $\sigma_{DG}^2 = \mathcal{O}(1)$ from Theorem 4.2, DG-PG achieves an ϵ -optimal policy in $T = \mathcal{O}\left(\frac{L}{\mu^2\epsilon} \log \frac{1}{\epsilon}\right)$ iterations, independent of N .*

Assumption G.1 (Smoothness and PL Condition). The cooperative objective $J(\boldsymbol{\theta})$ is L -smooth and satisfies the Polyak-Lojasiewicz (PL) condition with PL constant $\mu \in (0, L]$:

$$\frac{1}{2} \|\nabla J(\boldsymbol{\theta})\|^2 \geq \mu(J^* - J(\boldsymbol{\theta})),$$

where $J^* \triangleq \sup_{\boldsymbol{\theta}} J(\boldsymbol{\theta})$ denotes the optimal value of the cooperative objective.

Together, these conditions guarantee that stochastic gradient ascent achieves linear convergence of the optimality gap. These are standard conditions in stochastic optimization (Karimi et al., 2016), needed only to convert the $\mathcal{O}(1)$ variance bound (Theorem 4.2) into an explicit iteration complexity. They are commonly satisfied for smooth policy parameterizations such as softmax policies (Mei et al., 2020; Agarwal et al., 2021).

G.1. Proof of Theorem 4.3

Proof. Our proof first characterizes, through L -smoothness and the update rule, how the variance and bias of \hat{g}_{DG} affect the per-iteration change in J . We then apply the PL condition to connect the gradient norm $\|\nabla J\|^2$ to the optimality gap $J^* - J(\boldsymbol{\theta}_k)$, thereby obtaining the N -independent iteration complexity. The following analysis holds for a *fixed* mixing parameter $\alpha \in (0, 1)$. When α is varied dynamically in practice, the convergence guarantee applies to each phase as a snapshot analysis.

Step 1: Smoothness bound. Let $\bar{g}_{DG}(\boldsymbol{\theta}_k) \triangleq \mathbb{E}_k[\hat{g}_{DG}(\boldsymbol{\theta}_k)]$ denote the expected augmented gradient. Consider the stochastic gradient ascent update

$$\boldsymbol{\theta}_{k+1} = \boldsymbol{\theta}_k + \eta \hat{g}_{DG}(\boldsymbol{\theta}_k) \quad (24)$$

By L -smoothness of J :

$$J(\boldsymbol{\theta}_{k+1}) \geq J(\boldsymbol{\theta}_k) + \langle \nabla J(\boldsymbol{\theta}_k), \boldsymbol{\theta}_{k+1} - \boldsymbol{\theta}_k \rangle - \frac{L}{2} \|\boldsymbol{\theta}_{k+1} - \boldsymbol{\theta}_k\|^2.$$

Substituting $\boldsymbol{\theta}_{k+1} - \boldsymbol{\theta}_k = \eta \hat{g}_{DG}(\boldsymbol{\theta}_k)$ and taking the conditional expectation $\mathbb{E}_k[\cdot] \triangleq \mathbb{E}[\cdot | \boldsymbol{\theta}_k]$:

$$\mathbb{E}_k[J(\boldsymbol{\theta}_{k+1})] \geq J(\boldsymbol{\theta}_k) + \eta \langle \nabla J(\boldsymbol{\theta}_k), \bar{g}_{DG}(\boldsymbol{\theta}_k) \rangle - \frac{L\eta^2}{2} \mathbb{E}_k[\|\hat{g}_{DG}(\boldsymbol{\theta}_k)\|^2]. \quad (25)$$

Step 2: Per-iteration descent bound. The descent inequality Equation 25 shows that the per-iteration ascent on J is governed by two quantities: the inner product term $\langle \nabla J, \bar{g}_{DG} \rangle$, which captures the alignment between the true gradient and the augmented gradient, and the second moment term $\mathbb{E}_k[\|\hat{g}_{DG}\|^2]$, which captures the estimator's variance and bias. We bound both independently of N .

For the inner product term $\langle \nabla J(\boldsymbol{\theta}_k), \bar{g}_{DG}(\boldsymbol{\theta}_k) \rangle$, by definition of the expected augmented gradient:

$$\bar{g}_{DG}(\boldsymbol{\theta}_k) = (1 - \alpha) \nabla J(\boldsymbol{\theta}_k) - \alpha \nabla \mathcal{G}(\boldsymbol{\theta}_k).$$

Therefore:

$$\langle \nabla J(\boldsymbol{\theta}_k), \bar{g}_{DG}(\boldsymbol{\theta}_k) \rangle = (1 - \alpha) \|\nabla J(\boldsymbol{\theta}_k)\|^2 - \alpha \langle \nabla J(\boldsymbol{\theta}_k), \nabla \mathcal{G}(\boldsymbol{\theta}_k) \rangle.$$

Since improving J reduces the deviation \mathcal{G} (Assumption 3.2), the true gradients satisfy $\langle \nabla J(\boldsymbol{\theta}_k), \nabla \mathcal{G}(\boldsymbol{\theta}_k) \rangle \leq 0$, so $-\alpha \langle \nabla J, \nabla \mathcal{G} \rangle \geq 0$. Dropping this non-negative term yields the lower bound for the inner product term in Equation 25:

$$\langle \nabla J(\boldsymbol{\theta}_k), \bar{g}_{\text{DG}}(\boldsymbol{\theta}_k) \rangle \geq (1 - \alpha) \|\nabla J(\boldsymbol{\theta}_k)\|^2. \quad (26)$$

For the second moment $\mathbb{E}_k[\|\hat{g}_{\text{DG}}(\boldsymbol{\theta}_k)\|^2]$, by the bias-variance decomposition:

$$\mathbb{E}_k[\|\hat{g}_{\text{DG}}(\boldsymbol{\theta}_k)\|^2] = \|\bar{g}_{\text{DG}}(\boldsymbol{\theta}_k)\|^2 + \sigma_{\text{DG}}^2. \quad (27)$$

The variance $\sigma_{\text{DG}}^2 = \mathcal{O}(1)$ by Theorem 4.2. Since $\bar{g}_{\text{DG}} = (1 - \alpha)\nabla J - \alpha\nabla \mathcal{G}$, applying the triangle inequality:

$$\|\bar{g}_{\text{DG}}(\boldsymbol{\theta}_k)\|^2 \leq 2(1 - \alpha)^2 \|\nabla J(\boldsymbol{\theta}_k)\|^2 + 2\alpha^2 \|\nabla \mathcal{G}(\boldsymbol{\theta}_k)\|^2. \quad (28)$$

For the $\|\nabla \mathcal{G}(\boldsymbol{\theta}_k)\|$ term, by Equation 9 the gradient of the guidance term has the form $\nabla_{\theta^i} \mathcal{G} = \mathbb{E}[\langle \mathbf{x}_t - \tilde{\mathbf{x}}_t, \mathbf{z}_t^i \rangle \nabla_{\theta^i} \log \pi^i]$. Each factor is bounded:

- $\|\mathbf{x}_t - \tilde{\mathbf{x}}_t\|$ is bounded by compactness of the system state space.
- $\|\mathbf{z}_t^i\|$ is bounded because each agent has bounded marginal effect on the system state.
- $\|\nabla_{\theta^i} \log \pi^i\|$ is bounded by standard score function regularity.

Applying Cauchy–Schwarz to the inner product $\langle \mathbf{x}_t - \tilde{\mathbf{x}}_t, \mathbf{z}_t^i \rangle$ and combining with the score function bound, there exists a constant $B > 0$, independent of N , such that:

$$\|\nabla \mathcal{G}(\boldsymbol{\theta}_k)\| \leq B. \quad (29)$$

Combining Equations 29 and 28 with Equation 27, we obtain:

$$\mathbb{E}_k[\|\hat{g}_{\text{DG}}(\boldsymbol{\theta}_k)\|^2] \leq 2(1 - \alpha)^2 \|\nabla J(\boldsymbol{\theta}_k)\|^2 + 2\alpha^2 B^2 + \sigma_{\text{DG}}^2. \quad (30)$$

which is the upper bound for the second moment term in Equation 25.

Substituting the inner product bound (Equation 26) and the second moment bound (Equation 30) into the descent inequality (Equation 25), we obtain the per-iteration descent bound:

$$\begin{aligned} \mathbb{E}_k[J(\boldsymbol{\theta}_{k+1})] &\geq J(\boldsymbol{\theta}_k) + \eta(1 - \alpha) \|\nabla J(\boldsymbol{\theta}_k)\|^2 - \frac{L\eta^2}{2} (2(1 - \alpha)^2 \|\nabla J(\boldsymbol{\theta}_k)\|^2 + 2\alpha^2 B^2 + \sigma_{\text{DG}}^2) \\ &= J(\boldsymbol{\theta}_k) + [\eta(1 - \alpha) - L\eta^2(1 - \alpha)^2] \|\nabla J(\boldsymbol{\theta}_k)\|^2 - \frac{L\eta^2}{2} (2\alpha^2 B^2 + \sigma_{\text{DG}}^2). \end{aligned}$$

Under the update rule (Equation 24), for the gradient signal to contribute positively to the expected change in J , the coefficient of $\|\nabla J(\boldsymbol{\theta}_k)\|^2$ must be positive. Choosing $\eta \leq \frac{1}{2L(1-\alpha)}$ ensures $\eta(1 - \alpha) - L\eta^2(1 - \alpha)^2 \geq \frac{\eta(1-\alpha)}{2}$:

$$\mathbb{E}_k[J(\boldsymbol{\theta}_{k+1})] \geq J(\boldsymbol{\theta}_k) + \frac{\eta(1 - \alpha)}{2} \|\nabla J(\boldsymbol{\theta}_k)\|^2 - \frac{L\eta^2}{2} (2\alpha^2 B^2 + \sigma_{\text{DG}}^2). \quad (31)$$

Step 3: PL condition and recursion. We now use the PL condition to convert the gradient norm bound into optimality gap contraction.

Subtracting both sides of Equation 31 from J^* (Assumption G.1):

$$J^* - \mathbb{E}_k[J(\boldsymbol{\theta}_{k+1})] \leq J^* - J(\boldsymbol{\theta}_k) - \frac{\eta(1 - \alpha)}{2} \|\nabla J(\boldsymbol{\theta}_k)\|^2 + \frac{L\eta^2}{2} (2\alpha^2 B^2 + \sigma_{\text{DG}}^2).$$

Taking full expectation and defining $\Delta_k \triangleq \mathbb{E}[J^* - J(\boldsymbol{\theta}_k)]$:

$$\Delta_{k+1} \leq \Delta_k - \frac{\eta(1 - \alpha)}{2} \mathbb{E}[\|\nabla J(\boldsymbol{\theta}_k)\|^2] + \frac{L\eta^2}{2} (2\alpha^2 B^2 + \sigma_{\text{DG}}^2).$$

By the PL condition (Assumption G.1), $\mathbb{E}[\|\nabla J(\theta_k)\|^2] \geq 2\mu\Delta_k$. Substituting:

$$\Delta_{k+1} \leq (1 - (1 - \alpha)\mu\eta)\Delta_k + \frac{L\eta^2}{2}(2\alpha^2B^2 + \sigma_{\text{DG}}^2).$$

Unrolling this recurrence for T iterations by the geometric series formula:

$$\Delta_T \leq (1 - (1 - \alpha)\mu\eta)^T \Delta_0 + \frac{L\eta^2}{2}(2\alpha^2B^2 + \sigma_{\text{DG}}^2) \cdot \frac{1 - (1 - (1 - \alpha)\mu\eta)^T}{(1 - \alpha)\mu\eta}.$$

Since $\mu, \eta > 0$ and $\alpha \in (0, 1)$, we have $(1 - \alpha)\mu\eta > 0$. Combined with $\eta \leq \frac{1}{2L(1-\alpha)}$ and $\mu \leq L$ (Assumption G.1), this gives $(1 - \alpha)\mu\eta \in (0, \frac{1}{2}]$. Therefore $1 - (1 - (1 - \alpha)\mu\eta)^T \in (0, 1]$, which gives:

$$\Delta_T \leq (1 - (1 - \alpha)\mu\eta)^T \Delta_0 + \frac{L\eta}{2(1 - \alpha)\mu}(2\alpha^2B^2 + \sigma_{\text{DG}}^2). \quad (32)$$

To achieve $\Delta_T \leq \epsilon$, it suffices to bound both terms on the right-hand side of Equation 32 by $\epsilon/2$. For the second term, setting it equal to $\epsilon/2$:

$$\frac{L\eta}{2(1 - \alpha)\mu}(2\alpha^2B^2 + \sigma_{\text{DG}}^2) = \frac{\epsilon}{2} \implies \eta = \frac{(1 - \alpha)\mu\epsilon}{L(2\alpha^2B^2 + \sigma_{\text{DG}}^2)}.$$

For the first term, requiring $(1 - (1 - \alpha)\mu\eta)^T \Delta_0 \leq \frac{\epsilon}{2}$ gives:

$$T \geq \frac{1}{(1 - \alpha)\mu\eta} \log \frac{2\Delta_0}{\epsilon}.$$

Substituting the chosen η :

$$T \geq \frac{L(2\alpha^2B^2 + \sigma_{\text{DG}}^2)}{(1 - \alpha)^2\mu^2\epsilon} \log \frac{2\Delta_0}{\epsilon}.$$

The quantities L, μ, B, α , and $\sigma_{\text{DG}}^2 = \mathcal{O}(1)$ (by Theorem 4.2) are all independent of N . This simplifies to:

$$T = \mathcal{O}\left(\frac{L}{\mu^2\epsilon} \log \frac{1}{\epsilon}\right),$$

completing the proof. □

H. Cloud Scheduling Environment

We provide complete specifications of the cloud scheduling environment used in all experiments.

H.1. Physical Environment

Cluster Configuration. The cluster consists of N servers drawn from 12 heterogeneous instance types spanning three hardware generations, with configurations based on AWS instance types. Table 4 details the full configuration.

The efficiency parameters η_{CPU} and η_{Mem} model performance-per-watt differences across hardware generations. Gen-1 instances (circa 2015) have $\eta_{\text{CPU}} \in [0.70, 0.75]$, Gen-2 (circa 2017) have $\eta_{\text{CPU}} \in [0.84, 0.98]$, and Gen-3 (circa 2020+) have $\eta_{\text{CPU}} \in [1.06, 1.08]$. Job completion time scales as duration/ η_{CPU} , making high-efficiency servers more productive. Server types are sampled according to the specified weights and randomly shuffled across indices at scenario generation to prevent agents from exploiting positional patterns.

Workload Generation. We employ a *bimodal task distribution* reflecting real-world workload diversity:

- **CPU-intensive tasks** (~60% of arrivals): CPU requirement drawn from Pareto($\alpha = 1.7, x_m = 0.6$), clipped to $[0.5, 20]$ cores; memory requirement $m = c \cdot U(1.5, 3.0)$, clipped to $[0.5, 64]$ GB (low memory-to-CPU ratio).

Descent-Guided Policy Gradient

Table 4. Server instance types used in the simulation, based on AWS instance configurations.

Gen.	Instance Type	vCPUs	Memory (GB)	η_{CPU}	η_{Mem}	Weight
Gen-1	m4.8xlarge	32	128	0.70	0.68	10%
	t3.2xlarge	16	64	0.72	0.70	3%
	t3a.2xlarge	16	64	0.75	0.72	2%
Gen-2	m5.8xlarge	32	128	0.95	0.93	20%
	c5.18xlarge	64	128	0.98	0.93	10%
	c5.12xlarge	48	96	0.97	0.93	8%
	r5.8xlarge	32	256	0.87	0.92	9%
	r5.6xlarge	24	192	0.84	0.93	7%
	m5n.12xlarge	48	192	0.96	0.92	6%
Gen-3	m6i.8xlarge	32	128	1.06	0.95	15%
	c5n.18xlarge	64	256	1.08	0.95	8%
	c6i.32xlarge	96	384	1.08	0.96	2%

- **Memory-intensive tasks** ($\sim 40\%$ of arrivals): CPU requirement drawn from Pareto($\alpha = 2.2$, $x_m = 0.4$), clipped to $[0.2, 8]$ cores; memory requirement $m = c \cdot U(6, 12)$, clipped to $[1, 128]$ GB (high memory-to-CPU ratio).

All tasks share the same duration distribution: Log-normal($\mu = 3.0$, $\sigma = 0.5$), clipped to $[5, 150]$ timesteps, yielding mean duration ~ 20 timesteps with high variance.

The Pareto shape parameter $\alpha \in [1.7, 2.2]$ is calibrated to match the heavy-tailed resource demand distributions observed in the Google cluster trace (Reiss et al., 2011), where a small fraction of jobs consume disproportionate resources. The log-normal duration distribution is consistent with empirical observations from production clusters (Reiss et al., 2012). The bimodal CPU-to-memory ratio reflects the coexistence of compute-intensive (e.g., batch analytics) and memory-intensive (e.g., in-memory databases) workloads in modern data centers (Delimitrou & Kozyrakis, 2014).

Arrival Process. Jobs arrive according to a non-homogeneous Poisson process with time-varying intensity:

$$\lambda(t) = \bar{\lambda} \cdot \max\left(0.1, 1 + 0.3 \sin\left(\frac{2\pi t}{1000}\right) + \epsilon_t\right), \quad \epsilon_t \sim \mathcal{N}(0, 0.1)$$

where the base rate $\bar{\lambda}$ is calibrated via a capacity-aware formula to achieve target utilization $\rho \in [0.80, 0.85]$ across all scales. The sinusoidal term introduces a 1000-step tidal period, capturing the diurnal traffic patterns observed in production systems (Cortez et al., 2017), while ϵ_t adds stochastic perturbation.

H.2. Agent Interface

Each arriving job is handled by a dedicated agent whose decision is to select a target server for placement. At each timestep, multiple agents act concurrently, one per arriving job. The system has N servers, and we evaluate seven scales from $N=2$ to $N=200$.

Scale Configurations. Table 5 summarizes the experimental configurations. Each scale is defined by the number of servers N , the number of action-space clusters K , the number of servers per cluster $S = N/K$, and the target cluster utilization ρ used to calibrate the arrival rate $\bar{\lambda}$ (see Arrival Process above). Each episode consists of 3000 timesteps, with job arrivals during the first 2000 and the remaining 1000 reserved as a drain period.

Action Space. At small scales ($N \leq 20$), each agent directly selects one of the N servers ($K = N$, $S = 1$). At larger scales ($N \geq 50$), the action space grows prohibitively, so we partition servers into $K < N$ clusters of $S = N/K$ servers each, sorted by capacity (c_k^{CPU} , c_k^{Mem}) so that servers within each cluster have similar profiles. Each agent selects a *cluster* (action space of size K), and a deterministic Best-Fit heuristic assigns the job within the selected cluster to the server with the highest current utilization that still has sufficient free resources. If no server can accommodate the job, it is queued on the least-loaded server.

Table 5. Scale configurations for experimental evaluation. All scales use 200 training scenarios and 40 held-out test scenarios.

Scale	Servers (N)	Clusters (K)	Servers/Cluster (S)	Episode Length	Target Util. (ρ)
tiny	2	2	1	3000	[0.80, 0.85]
small	5	5	1	3000	[0.80, 0.85]
compact	10	10	1	3000	[0.80, 0.85]
standard	20	20	1	3000	[0.80, 0.85]
medium	50	25	2	3000	[0.80, 0.85]
heavy	100	25	4	3000	[0.80, 0.85]
xlarge	200	40	5	3000	[0.80, 0.85]

Observation Space. For scales $N \leq 100$, each agent receives a $(7N + 2N_{\text{agents}} + 4)$ -dimensional observation consisting of:

- **Global server state** ($7N$ dims): For each server $k \in \{1, \dots, N\}$, we include normalized CPU utilization, memory utilization, local queue length (clipped at 50), CPU efficiency, memory efficiency, CPU capacity, and memory capacity.
- **All task information** ($2N_{\text{agents}}$ dims): Normalized CPU and memory requirements for all concurrently dispatched jobs (CTDE-style global information).
- **Job features** (2 dims): Normalized CPU and memory requirements of this agent’s assigned job.
- **Temporal feature** (1 dim): Normalized timestep t/T_{max} .
- **Agent identifier** (1 dim): Normalized agent index, used with a learnable embedding (see below).

Observation Compression ($N \geq 200$). Since the agent’s action selects a *cluster* rather than a specific server, per-server detail is unnecessary at large scales. For $N \geq 200$ (cluster size $S = N/K \geq 5$), we compress per-server states into *cluster-level sufficient statistics*: each cluster is represented by a 28-dimensional vector comprising CPU utilization quantiles (min, Q25, median, Q75, max, mean, std), memory utilization quantiles (7 dims), CPU-memory joint distribution features (correlation, fraction CPU-/memory-heavy/balanced; 4 dims), queue congestion statistics (total, max, mean, std, fraction non-empty; 5 dims), and capacity-efficiency features (free CPU/memory fractions, mean efficiency, cluster size, overloaded fraction; 5 dims). Task information is similarly compressed to 6 dimensions (mean, std, max for CPU and memory demands). The total observation dimension becomes $28K + 10$, achieving up to $6.4\times$ reduction compared to the raw representation while preserving all scheduling-relevant information. The DG-PG guidance signal is always computed on raw server states and is unaffected by this compression.

Agent ID Embedding. To enable parameter sharing across heterogeneous agents, we embed each agent’s normalized index via a learnable `nn.Embedding` layer (dimension 16), which is concatenated with the remaining observation features before the first hidden layer. This allows a single shared network to learn agent-specific behaviors.

H.3. Reward Function

The shared reward signal is a weighted combination of two objectives:

$$r_t = - \left(w_1 \cdot \underbrace{\frac{Q_{\text{global}}(t) + \sum_{k=1}^N Q_k(t)}{N}}_{\text{Queue Penalty (Latency)}} + w_2 \cdot \underbrace{\frac{\sum_{k=1}^N \frac{L_k(t)}{\eta_k}}{C_{\text{total}}}}_{\text{Energy Penalty}} \right)$$

where $Q_{\text{global}}(t)$ is the global buffer size, $Q_k(t)$ is the local queue at server k , $L_k(t)$ is the workload (CPU + memory) at server k , η_k is the server’s efficiency, and C_{total} is the total cluster capacity. We set $w_1 = 1$ and $w_2 = 20$ so that both penalties contribute comparably to the reward. Without the multiplier, the queue penalty typically ranges in $[0, 20]$, whereas the normalized energy ratio remains below 1. Load-balancing (utilization variance) is handled entirely by the DG-PG guidance signal and is therefore excluded from the reward.

I. Training Configuration

All methods are trained with PPO using parameter sharing across agents. We use two model classes: neural network (NN) models for DG-PG, and linear models for the three-way comparison, because MAPPO and IPPO cannot converge with NN models in our environment (Section J).

For the hyperparameter selection (Section 6.2) and scalability experiments (Section 6.4), DG-PG is trained with NN models covering $N=5$ to $N=200$. We initially attempted to train MAPPO and IPPO with the same NN architecture, but they failed to converge across ~ 20 configurations at $N=5$ and $N=2$ (Section J). To enable a fair comparison despite this failure, the controlled comparison (Section 6.3) uses linear models for all three methods at $N \in \{2, 5, 10\}$. Linear models ($\pi(a|s) = \text{softmax}(Ws + b)$, $V(s) = w^\top s + b$) cannot overfit and have a convex critic loss, making split-epoch training (see below) effective where it failed with NN. DG-PG also uses linear models in this comparison, so any performance difference is attributable solely to the guidance signal.

I.1. Shared Hyperparameters

The following parameters are identical across all methods and both model classes:

- Discount factor: $\gamma = 0.99$
- GAE parameter: $\lambda = 0.95$
- PPO clipping ratio: $\epsilon = 0.2$ (except NN at $N \geq 50$; see below)
- Optimizer: Adam with separated actor-critic updates and independent gradient clipping
- Value loss: Huber loss ($\delta = 10.0$) instead of MSE, reducing sensitivity to reward outliers
- Return normalization: target returns standardized (zero mean, unit variance) per minibatch
- Learning rate decay: linear decay to 1% of the initial value over 90–95% of training

I.2. Linear Models (Controlled Comparison)

For the controlled comparison at $N \in \{2, 5, 10\}$, all three methods share the same linear architecture and the same core training parameters. Table 6 lists the full configuration.

Several shared parameters above the midline were set to stabilize MAPPO and IPPO, based on the tuning documented in Section J:

- **Split-epoch training** (critic 20 epochs, actor 3 epochs): MAPPO and IPPO require a well-trained critic before the actor receives meaningful advantage signals. A single linear layer needs many gradient steps to fit the value function; without this asymmetric schedule, advantage estimates are too noisy for stable policy updates.
- **Large mini-batch** (10,000) and **high rollout count** (24): With smaller batches (e.g., 256–1,024), MAPPO and IPPO exhibit wildly oscillating rewards that never converge. Multi-agent policy gradients in this environment have high variance due to heterogeneous servers, bimodal workloads, and non-stationary arrivals, requiring large batches to average over noise.

These measures build on the official MAPPO configuration (Yu et al., 2022) with further stabilization. DG-PG uses the same settings for fair comparison.

The remaining differences below the midline each favor the baselines:

- **Entropy**: MAPPO/IPPO use a fixed coefficient (0.005) rather than decay, because entropy decay caused premature policy collapse in our tuning. The fixed value was selected as the best-performing setting across grid search.
- **Training length**: MAPPO/IPPO are trained for 500 episodes ($2.5\times$ longer than DG-PG’s 200), providing additional convergence time.

Table 6. Hyperparameters for linear model experiments (Section 6.3). Parameters above the midline are shared across all methods; those below differ.

Parameter	Value
Model class	Linear (single layer, no hidden units)
Learning rate	1×10^{-3} (linear decay to 1%)
Discount factor γ	0.99
GAE λ	0.95
PPO clipping ϵ	0.2
Critic epochs / Actor epochs	20 / 3 (split-epoch)
Mini-batch size	10,000
Gradient clipping	max norm 10.0
Huber loss δ	10.0
Parallel environments	4
Rollouts per episode	24
DG-PG entropy coefficient	0.01 (exponential decay to 10^{-4})
MAPPO / IPPO entropy coefficient	0.005 (fixed, no decay)
DG-PG training episodes	200
MAPPO / IPPO training episodes	500
DG-PG α schedule	Same as NN (0.9 \rightarrow 0.2)

I.3. Neural Network Models (DG-PG)

The NN architecture consists of a 2-layer MLP with Tanh activations for both actor and critic, plus a learnable agent-ID embedding (dimension 16) concatenated with the observation. This configuration is shared by the hyperparameter selection (Section 6.2) and scalability experiments (Section 6.4).

DG-PG Hyperparameters.

- Learning rate: 3×10^{-4} (exponential decay)
- Initial entropy coefficient: 0.02 (exponential decay to 10^{-4})
- PPO update epochs: $K = 4$ (unified for actor and critic)
- Training episodes: 200
- Gradient clipping: max norm 0.5
- Guidance weight α follows a dynamic three-phase schedule (Section 6.2): $\alpha = 0.9$ for the first 10% of training, linear decay 0.9 \rightarrow 0.2 from 10% to 50%, and $\alpha = 0.2$ thereafter
- Signal normalization: running mean and variance (momentum 0.99), clipped to $[-3, 3]$

Scale-Specific Settings. Network capacity and mini-batch sizes are scaled with problem size. At large scales ($N \geq 50$), we widen the PPO clipping ratio to $\epsilon = 0.4$ because the larger number of parameters makes the model robust to more aggressive updates. Table 7 provides the complete settings.

Training Stability. The guidance signal fundamentally changes DG-PG’s training dynamics. By reducing gradient variance (Theorem 4.2), it eliminates the need for the stabilization measures that MAPPO and IPPO require. *Batch size and rollouts:* DG-PG trains with mini-batches of 256–2048 and 4–12 rollouts, an order of magnitude smaller than the linear experiments, yet its actor-critic updates remain stable without split-epoch scheduling or large-batch averaging. *α schedule:* when α is large (early training), the strong guidance drives rapid convergence; when α is small (late training), the inherently stable updates allow the critic to continue learning effectively, without the actor-critic oscillation observed in MAPPO and IPPO. *No return normalization:* DG-PG trains stably without return normalization. This preserves meaningful reward differences across scenarios (e.g., -80 vs. -100) that normalization would otherwise collapse.

Descent-Guided Policy Gradient

Table 7. Scale-specific hyperparameters for NN models (DG-PG only).

Servers (N)	Hidden Dim	Mini-batch	Rollouts	Parallel Envs	ϵ
5	128	256	12	4	0.2
10	128	512	12	4	0.2
20	128	512	12	4	0.2
50	256	1024	8	4	0.4
100	512	2048	6	2	0.4
200	1024	2048	4	1	0.4

J. Baseline Failure Analysis

MAPPO and IPPO fail to learn competitive policies with neural network models due to a fundamental *actor-critic update frequency dilemma*: the actor and critic have conflicting requirements for gradient update frequency, and no configuration resolves both simultaneously. We verified this across ~ 20 training runs at $N=5$ and $N=2$, varying batch size, update epochs, entropy coefficient, value normalization, gradient clipping, and model architecture (NN and linear). Table 8 lists the representative runs at $N=5$ with a 2-layer MLP (128 hidden units).

Table 8. Representative NN MAPPO runs at $N=5$. “Steps/ep” = total gradient updates per episode.

Run	Key Change	Batch	K -epochs	Steps/ep	c_{ent}	Eps	Best Rew	Failure Mode
0	DG-PG defaults	256	4	3,064	0.02 (decay)	726	-87	Entropy collapse (1.59 \rightarrow 0.26)
1	+ValueNorm	256	10	7,660	0.01	58	-78	Entropy collapse (1.60 \rightarrow 0.88)
2	K : 10 \rightarrow 4	256	4	3,064	0.01	73	-80	Slow entropy collapse (1.54 \rightarrow 1.36)
3	c_{ent} : 0.01 \rightarrow 0.03	256	4	3,064	0.03	176	-92	Entropy bonus drowns advantage
4	Align to official	50,000	10	40	0.01	170	-71	Critic too slow (ExplVar \leq 0.30)
5	Batch: 50K \rightarrow 20K	20,000	15	150	0.01	95	-77	Critic still insufficient
6	Batch: 20K \rightarrow 10K	10,000	15	300	0.01	1,000	-57	No convergence; eval -198
7	+PBRS shaping	10,000	15	300	0.01	164	-80	Shaping signal $<$ 0.001% of reward

J.1. The Update Frequency Dilemma

The table reveals three regimes, each failing for a different reason:

- **High frequency** (Runs 0–3; 3,000+ steps/ep): The critic learns well (explained variance reaches 0.7), but the actor undergoes entropy collapse, converging to a near-deterministic, suboptimal action within 50–70 episodes, after which performance degrades irreversibly.
- **Low frequency** (Runs 4–5; 40–150 steps/ep): Entropy remains stable, but the critic receives too few updates to learn accurate value estimates (explained variance \leq 0.30), leaving the actor with uninformative advantages.
- **Intermediate frequency** (Run 6; 300 steps/ep): The best compromise, with entropy stable and critic explained variance reaching 0.35–0.49, but training rewards oscillate between -57 and -135 over 1,000 episodes with no convergence trend. Evaluation on 40 held-out scenarios yields -198, far worse than the Random baseline (-84.2).

J.2. Attempts to Break the Dilemma

We tested four structural modifications, none of which resolved the fundamental conflict:

ValueNorm (Yu et al., 2022). Exponential moving average statistics ($\beta=0.99999$) improved critic learning (explained variance from 0.0 to 0.7) but did not prevent entropy collapse at high frequencies or slow critic convergence at low frequencies.

Official MAPPO alignment (Run 4). We aligned 7 hyperparameters with the official implementation (Yu et al., 2022): mini-batch size (256 \rightarrow 50,000), value loss coefficient (0.5 \rightarrow 1.0), Huber δ (1.0 \rightarrow 10.0), gradient clipping (0.5 \rightarrow 10.0), fixed entropy, and increased rollouts (12 \rightarrow 24). This eliminated entropy collapse by reducing gradient steps from 3,064 to 40 per episode, but made the critic too slow.

Potential-based reward shaping (Run 7). PBRs with $\Phi(s) = -\text{Var}(\text{utilization})$ produced negligible shaping signals, with $|\gamma\Phi(s') - \Phi(s)| \approx 0.0003$ versus rewards of magnitude 60–140. The bottleneck is gradient variance (cross-agent credit assignment), not temporal credit assignment.

Asynchronous actor-critic ($N=2$). Separate critic-then-actor optimization at the smallest scale showed near-zero KL divergence and 0% PPO clipping, confirming that the gradient signal is too noisy for meaningful policy updates even with only 2 agents.

J.3. Transition to Linear Models

The dilemma is fundamentally harder for neural networks. A high-capacity critic can memorize recent scenarios but fails to generalize, while the actor’s non-convex loss landscape makes it prone to entropy collapse. Linear models ($\pi(a|s) = \text{softmax}(Ws + b)$, $V(s) = w^\top s + b$; ~ 70 parameters) resolve this because they cannot overfit, and their convex critic loss permits more update epochs without instability. Even so, MAPPO and IPPO still require additional stabilization, including split-epoch training, large mini-batches, and elevated rollout counts, as detailed in Section I. This isolates gradient variance as the sole remaining variable, providing the strictest test of DG-PG’s contribution.

These failures are consistent with the $\Theta(N)$ gradient variance scaling analyzed in Section 2. Three environment-specific factors further amplify the difficulty:

- *Server heterogeneity* ($\eta_{\text{CPU}} \in [0.70, 1.08]$): The optimal policy changes substantially across scenarios, preventing the critic from learning a single value function that generalizes.
- *Non-stationary arrivals*: Poisson processes with time-varying rates make each episode structurally different, so the critic cannot rely on patterns from previous episodes.
- *Bimodal workloads*: Jobs arrive with two distinct resource profiles, producing multimodal reward distributions that further increase gradient variance per sample.

Together, these factors compound the $\Theta(N)$ variance scaling and make this environment particularly challenging for standard multi-agent policy gradient methods.

K. Computational Resources

All experiments were conducted on a single Apple M1 chip (8-core CPU, 16 GB unified memory, circa 2021) using CPU-only computation, without any GPU acceleration.

Convergence speed. A key practical advantage of DG-PG is its rapid convergence. As shown in Table 9, DG-PG reaches near-optimal performance within approximately 10 episodes across *all* scales, after which further training yields only marginal refinement.

Time breakdown. Each training episode has two phases: environment rollout (simulating N agents for 3000 timesteps) and policy optimization (gradient updates on the collected experience buffer of $N \times 3000$ transitions). As N grows, the optimization phase increasingly dominates wall-clock time, rising from 42% at $N=5$ to 66% at $N=100$, because the buffer size scales linearly with N . All timing results were obtained on consumer-grade hardware without GPU acceleration. Wall-clock times would decrease significantly with GPU-based batch gradient computation.

Table 9. DG-PG convergence analysis on Apple M1 (CPU-only). “Convergence” is defined as the episode at which reward first reaches within 10% of the best observed reward.

Agents (N)	Converge Ep	Converge Time	Per-Episode	Total (200 ep)
5	≤ 5	~ 45 s	~ 9 s	~ 0.5 hr
10	≤ 5	~ 1 min	~ 12 s	~ 0.7 hr
20	≤ 10	~ 3 min	~ 20 s	~ 1.1 hr
100	≤ 10	~ 25 min	~ 2.5 min	~ 8 hr
200	≤ 10	~ 35 min	~ 3.5 min	~ 12 hr